The Quantification of Radiation Induced Pulmonary Fibrosis

By

Li Ming Wang

Department of Experimental Medicine

McGill University

Montreal, Quebec, Canada

August 2019

A thesis submitted to McGill University in partial fulfillment of the requirements of the degree of

Master of Science (M.Sc.) in Experimental Medicine

"Swing da man da sheetaz"

- Tyco Tump-Hard

Table of Contents

Abbreviations

3D	Three-Dimensional
3D-CRT	Three-Dimensional Conformal Radiation Therapy
CBCT	Cone-Beam Computed Tomography
CI	Confidence Interval
COPD	Chronic Obstructive Pulmonary Disease
CT	Computed Tomography
CTCAE	Common Terminology for Adverse Events
CTV	Clinical Target Volume
DNA	Deoxyribonucleic Acid
ECM	Extra-Cellular Matrix
EORTC	European Organization for Research and Treatment of Cancer
FDA	Food and Drug Administration
FEV	Forced Expiratory Volume
GM-CSF	Granulocyte-Macrophage Colony Stimulating Factor
GTV	Gross Tumor Volume
Gy	Gray
H&E	Hematoxylin & Eosin
HSB	Hue, Saturation and Brightness
HU	Hounsfield Unit
IMRT	Intensity Modulated Radiotherapy
IR	Ionizing Radiation
LENT-SOMA	Late Effects in Normal Tissue – Subjective Objective Management Analysis

MLD	Mean Lung Dose
MSC	Mesenchymal Stem Cell
OAR	Organs At Risk
PBS	Phosphate-buffered Saline
PEF	Peak Expiratory Flow
PRV	Planning Risk Volume
PSEF	Pulmonary Segment Equivalent of Fibrosis
PTV	Planning Target Volume
RILF	Radiation Induced Lung Fibrosis
RIPF	Radiation Induced Pulmonary Fibrosis (interchangeable with RIPF)
ROI	Region of Interest
RT	Radiotherapy
RTOG	Radiation Therapy Oncology Group
SABR	Stereotactic Ablative Radiotherapy
SBRT	Stereotactic Body Radiation Therapy
TGF-ß	Transforming Growth Factor Beta
TNFα	Tumor Necrosis Factor alpha
VMAT	Volumetric Modulated Arc Therapy

Abstract

Radiation induced pulmonary fibrosis (RIPF) is a late and permanent complication of thoracic radiotherapy. It is characterized by the formation of permanent scar tissue in the lungs, often reducing the already depleted pulmonary reserves and decreased pulmonary function of lung cancer patients. Currently, the assessment of RIPF is dependent on the qualitative and subjective appraisals of physicians, evaluated only after patient self-reports, despite RIPF presenting asymptomatic in many cases. As a result, RIPF is poorly identified and assessed with high variability. Recent studies have suggested that quantifying traditionally qualitative diagnostic outcomes, such as visually appraised RIPF, can yield a more replicable and objective scoring. In this work, we explore the quantification of RIPF in an animal (rat) model through the use of histology and in a prospective clinical study using patient computed tomography imaging as a surrogate for traditional qualitative appraisals. We validated two quantitative models, which analyse specific volumes of a given color in histology and the extent of a given radio-density in computed tomography imaging, in the context of two clinically relevant problems and compared the performance of our quantitative methods to that of physicians. In the animal model, the area of Masson's Trichrome stained regions of blue, indicative of fibrosis was used as a quantitative surrogate for fibrosis scoring. In the prospective patient study, the volume of space occupied by an empirically determined Hounsfield Unit range, deemed to be the density range for fibrosis, is used as a quantitative surrogate for fibrosis scoring. These quantitative methods showed promise as a capable, objective and reproducible method of scoring RIPF. However, quantifying a single feature such as color or radio-densities is not enough. For RIPF, a quantitative component which specifically analyzes structural changes due to RIPF is necessary in order to produce more physician-like performance. Techniques which can quantify anatomical damage, such as the change in anatomical structures or overall distortion of anatomical entities, can further improve the quantitative technique and simulate the variety of additional features that physicians take into account. The method

in its current state is still capable of being applied for future studies of RIPF to generate more consistent and objective outcomes for analysis.

Résumé

La fibrose pulmonaire causée par la radiothérapie (FPPR) est une complication tardive et permanente de la radiothérapie thoracique. Elle est caractérisée par le développement de tissus cicatriciels permanents aux poumons des patients traités pour le cancer du poumon, qui présentent déjà un réserve et fonction pulmonaire réduit. Présentement, l'évaluation de la FPPR dépend des examens qualitatifs et subjectifs fait par les médecins et souvent cette évaluation n'est pas faite sauf si les patients signalement des symptômes, la FPPR est généralement asymptomatique. La FPPR est présentement mal identifiée et elle évaluée avec une grande variabilité. Les études récentes suggèrent que quantifier des résultats diagnostiques qui sont traditionnellement qualitatives, comme par exemple l'évaluation visuelle de la FPPR, peut produire un système de notation plus objectif et reproductible. Dans cette étude, on explore la quantification de la FPPR chez un modèle animal (rat) en utilisant l'histologie et dans une étude clinique prospective, en utilisant l'imagerie de la tomodensitométrie de patients avec l'objectif de remplacer les évaluations traditionnellement qualitatives. On a validé deux modèles quantitatifs qui analysent des volumes spécifiques d'une couleur spécifique en histologie et la mesure d'une radio-densité spécifique avec l'imagerie de la tomodensitométrie dans le cadre de deux études cliniques pertinentes et on a comparé les résultats de nos méthodes quantitatives à ceux des médecins. Chez le modèle animal, les régions du poumon colorées en bleu avec la coloration Trichrome de Masson, indiquant la fibrose, ces régions sont utilisées pour quantifier la fibrose. Dans l'étude prospective avec des patients, le volume de l'espace occupé par une gamme de Hounsfield Unit définie empiriquement, qui est considérée une gamme de la fibrose, est utilisée pour quantifier la fibrose. Ces méthodes quantitatives se sont révélées prometteuses comme système de cotation de la FPPR, et sont compétents, objectifs et reproductibles. Par contre, la quantification des caractéristiques comme la couleur et la radio-densité ne sont pas assez pour évaluer complètement la FPPR. Pour la FPPR, il est primordial d'utiliser une composante quantitative qui analyse spécifiquement les changements

structurels causés par la FPPR afin de reproduire un résultat similaire à l'évaluation d'un médecin. Les techniques qui peuvent quantifier les dommages anatomiques, dont les changements structurels anatomiques et la déformation d'entités anatomiques, peuvent améliorer davantage les résultats des autres techniques quantitatives et peuvent simuler une plus grande variété de caractéristiques que celles qui sont considérés par les médecins. La méthode dans son état actuel est apte pour être utiliser dans des études futures de la FPPR, afin de générer des résultats plus cohérents et objectifs à analyser.

Acknowledgements

I like to, first and foremost, thank my supervisor, Dr. Norma Ybarra, for her continued mentorship and teaching. Having worked with her for close to 5 years, many of my positive dispositions as a student and academic are due to her tutelage. She has always afforded me her time and energy, giving me space to explore, while making research exciting and fun, but also keeping me rigorous and dedicated. And for that I am truly grateful.

Secondly, I like to thank Dr. Jan Seuntjens and Dr. Avishek Chatterjee, and the past and current members of the Medical Physics Unit who continue to give me guidance and assist me throughout my journey over the years. Special thanks to Dr. Issam El Naqa, who also continues to remain an accessible mentor despite being at the University of Michigan.

I would also like to thank Dr. Alexandre Semionov, Dr. Sergio Faria, Dr. James Tsui and many other members of the clinical staff and residents at the Royal Victoria Hospital, the Cedar's Cancer Center and the Montreal General Hospital that I've had the pleasure of collaborating with. They've been tremendous help in providing the necessary clinical perspective that vital to the completion of this thesis.

Furthermore, I would like to thank the members of my thesis committee who have not been mentioned thus far; Dr. Alain Nepveu and Dr. Stephane Laporte. Both of whom provided valuable guidance in the writing of this thesis, experience in the completion of my Masters degree and advice for my future aspirations.

A special thanks to Dr. Anita Parmar, Mr. David "Jhave" Johnston and the members of McGill's Building 21 for giving a home to my crazy ideas and supporting me in my efforts to broaden my horizons as a researcher, allowing me to explore the things that I don't always get funded for. My

appreciation also goes out to the professors, course administrators and formers students of the Biology Department at McGill University who have allowed me to develop my teaching abilities and who continue to trust in my abilities to mentor the next generation of student.

And finally, the warmest and greatest thanks to my mother, Molin Fu, my father, Jiancai Wang, my extended family, my girlfriend, Michelle Brais, and my friends for helping me stay afloat amidst this crazy world. Without the sum total of all these individuals, I could not be where I am today. Their continued support has given me the fearlessness to chase my dreams and give my all day in and day out.

Preface

Statement of Originality

I certify that the intellectual content of this thesis is the product of my own work and that all the assistance received, sources cited, and collaborators worked with in preparing this thesis have been acknowledged. This thesis has also not been submitted for the attainment of any other degrees.

The two manuscripts included within the contents of the thesis have been submitted for publication in journals as original literature and are also the product of my own work in collaboration with the authors listed.

Contributions of Authors

Dr. Alexandre Semionov – assisted in developing the method for qualitative RIPF appraisal, training the physician collaborators to perform fibrosis scoring and providing revisions and comments for the final submitted manuscript.

Dr. Avishek Chatterjee – assisted in developing the statistical methods and providing the revisions and comments for the final submitted manuscripts.

Dr. Sangkyu Lee – build the initial algorithm for the automated quantification of fibrosis, for use with rat models of disease, provided quality assurance on treatment plans for the animal experiments and provided revisions and comments for the final submitted manuscripts.

Dr. James Tsui – assisted in ideating the basis for calculating the image correction factor and provided revisions and comments for the final submitted manuscript.

Dr. Issac Yang & Dr. Yarab Al Bulushi – collaborators on the second manuscript tasked with the fibrosis scoring outlined as well as providing revision and comments for the final submitted manuscript.

Dr. Sungmi Jung – certified pathologist tasked with scoring the rat fibrosis samples and provide revisions and comments for the final submitted manuscript.

Mrs. Monica Serban – created the animal treatment plans for the experiment using a rat model.

Mrs. Krishinima Jeyaseelan – extensively assisted in preparing the rats throughout the duration of the animal study.

Dr. Issam El Naqa – generated the initial outline for the animal study.

Dr. Jan Seuntjens – offered extensive experience and direction to the publication of both manuscripts and provided revisions and comments for the final submitted manuscripts.

Dr. Norma Ybarra – supervisor of thesis work and provided extensive support, revision and teaching for both the writing of the thesis and the two submitted manuscripts. Also contributed to the animal experimentation portion performing the cell administrations and preparation of the rats.

List of Tables

List of Figures

§1 Introduction

1.1 – Radiation Induced Pulmonary Fibrosis (RIPF)

Ionizing Radiation and Radiotherapy

Since the discovery of the X-Ray by Wilhelm Röntgen, at the end of the 19th century, the destructive capabilities of ionizing radiation (IR) have been harnessed for therapeutic uses. Specifically, it was recognized as a powerful means of treating maladies such as cancers. Its ability to kill cells and disrupt biomolecular function from afar, without the need for invasive surgery, offered a unique opportunity to change how ablative medical procedures are performed. Now in the 21st century, there are 14 million cases of cancer diagnosed annually, with 50% these cases being able to benefit from radiotherapy (RT). Currently, over 61% of lung cancer patients are referred for radiotherapy treatment [1].

However, despite the popularity of RT as a non-invasive treatment, there is still much research invested into maximizing its therapeutic benefits. IR is indiscriminately destructive and will actively destroy cells whether they are cancerous or not. As such, development of modern RT revolves around maximizing radiation deposition in the tissues of interest, or target tissues, such as cancer cells and cancerous tumors, while reducing IR deposition in surrounding healthy tissues, often designated as organs at risk (OAR) [2, 3]. Balancing these two characteristics ensures that a precise amount of IR is used to destroy the targeted cells and tissues, improving tumor control in the case of treating solid tumors, while minimizing the exposure of healthy cells and tissues, reducing the likelihood of adverse reactions and toxicities.

Much of this optimization between maximizing dose to targets and minimizing dose to healthy tissues is currently carried out through automated planning and calculation. Beginning with a stack of

computed tomography (CT) images, which forms a three-dimensional (3D) CT volume, of the region of interest, local landmarks are contoured to delineate and outline the necessary targets for treatment as well as important OARs (Figure 1.1.1). Physicians are tasked with identifying and outline both a gross tumor volume (GTV) – which delineates the exact boundaries of the solid tumor in question – and a clinical target volume (CTV) – which delineates the boundaries for all volumes which require a dose of IR, such as the tumor bed, or adjacent lymph nodes with identified cancer properties. An additional increase in the size of the CTV, to account for uncertainty due to shifts in the position of the CTV due to movement, is applied to create the planning target volume (PTV), a region which a radiation dose will be deposited. A treatment plan is computed using dose requirements for the PTV, CTV and GTV while respecting the maximum tolerable doses for delineated OARs (Figure 1.1.2). This optimization ultimately ensures that treatment regions receive as much dose as possible while the regions of healthy tissue, receive as little dose as possible.

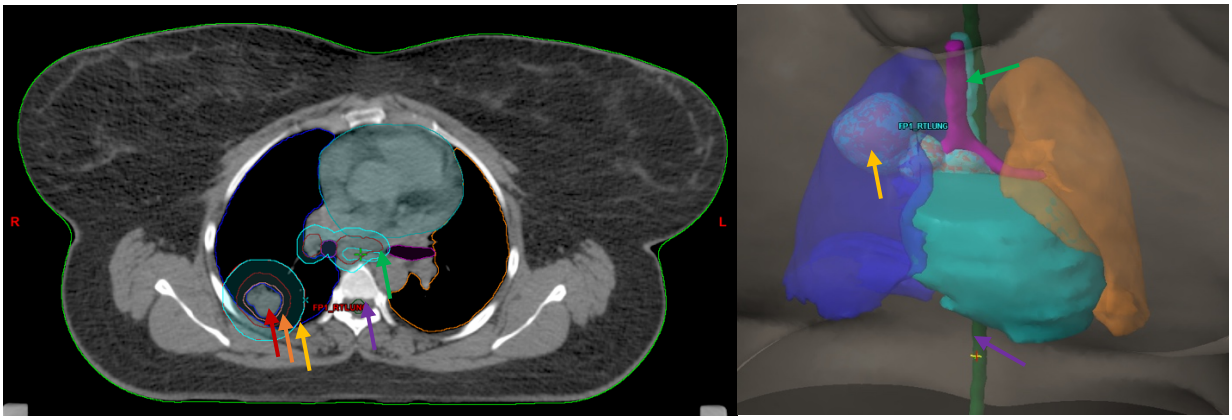

Figure 1.1.1 – Image take from our patient database. Contours or outlines of OARs in a 2-dimensional (2D) CT slice (left) and in a 3D volume (right). The PTV (yellow arrow), CTV (orange arrow) and GTV (red arrow) can be visualized in both images. Several organs at risk can also be visualized, including the heart (teal outline/volume), left lung (orange outline/volume), right lung (blue outline/volume), carina (magenta outline/volume), esophagus (green arrow) and spinal cord (purple arrow).

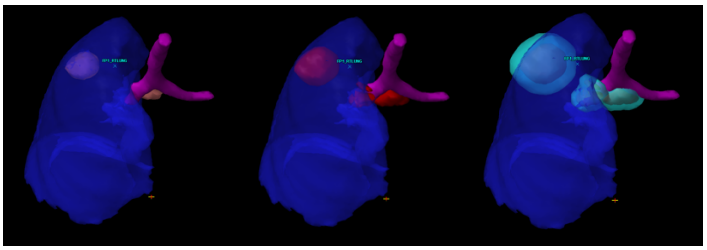

Figure 1.1.2 – Image take from our patient database, depicting the size differences between the GTV (leftmost image), CTV (middle image) and PTV (rightmost image) in relation to surrounding anatomical structures and OARs.

In order to further optimize radiation dose deposition in target and non-target volumes, there are many specialized RT techniques used to increase the conformity of radiation fields to the PTV. Conventionally, the most widely used modality of RT is three-dimensional conformal RT (3D-CRT) which fits the shape of a radiation field to the projection of the 3D image of a tumor [3]. This modality is often paired with chemotherapy with cytotoxic drugs such as carboplatin, taxol or gemcitabine for better disease control of stage III non-small cell lung cancers (NSCLC) [4, 5]. However, in cases where the PTV is of an odd shape, containing concave curvature, or surrounded by structures that have greatly reduced radiation tolerance, other techniques which can render more conformal and precise fields are used. The first of such techniques is intensity-modulated radiation therapy (IMRT) which makes use of adaptive beam intensities. The beams change intensities when they intersect with OARs, to more conformally deposit dose to the PTV and reduce dose exposure to OARs [3, 6, 7]. Alternatively, there is SBRT which utilizes a 360^{o} rotating accelerator to deliver a small precise beam over an arc of movement, reducing or completely removing the need for the intersection of beam tracks with OARs [3, 7-9]. This technique also allows for the building of much more conformal dose deposition in addition to reduced dose fractionation due to the use of larger doses per fraction [3]. Both the IMRT and SBRT technique are widely applied modalities in frail patients who cannot undergo surgery or endure the intensity of a chemotherapeutic or a concomitant regiment involving

RT. SBRT specifically is often used in early stage tumors, as the greater conformality, high dose per fraction and reduced fractionation allows SBRT to better treat smaller targets without the need for concomitant chemotherapy to achieve similar levels of disease or tumor control [10]. On the other hand, IMRT is often used in the treatment of head and neck cancer where the sparing of small radiosensitive organs such as salivary gland and optic nerves is desired [11]. Examples of the treatment plan for the three treatment modalities are presented in Figure 1.1.3. Despite conformal modalities being much more effective at sparing healthy tissues surrounding the primary disease, the application of these techniques in the lung, and for NSCLC, is still immature due to respiratory motion during treatment delivery [12, 13].

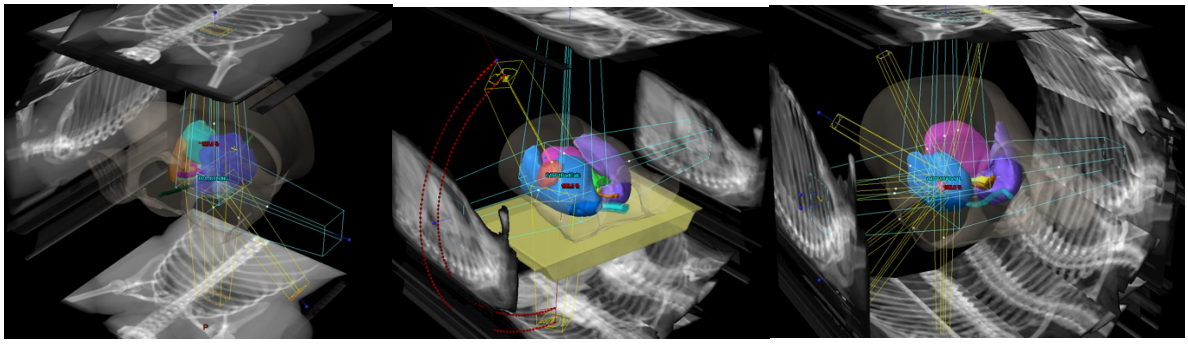

Figure 1.1.3 – Image taken from our patient database showing 3D-CRT (left), IMRT (middle) and SBRT (right) treatment plans with the beam tracks to be applied and the OARs involved.

Pulmonary Fibrosis

Pulmonary fibrosis is a class of diseases characterized by the excess formation of fibrous connective tissue in the lung. In most cases, the formation of connective tissue is akin to a permanent scar formation, due to either chemical, physical or biological insults that causes sustained damage, cell death and chronic cellular apoptosis [2, 14]. This process of sustained cell damage and death leads to replacement of loco-regional cells, tissues and structures with a combination of stable and permanent collagen type-I and collagen type-III that is not structurally organized or functional [15]. The fibrous

scar tissue replaces many of the damaged or dead healthy tissue in the region of insult, as a result of prolonged inflammation in response to cell death and tissue damage. The deposited scar tissue, in mild cases of fibrosis, only thickens the alveolar walls and walls of the interstitial structures of the lung, reducing the elasticity of the lung. In more severe cases the deposited scar tissue completely replace any semblance of specialized tissues and structures and overall does not contribute to the oxygen exchange function of the lungs [2, 14, 16].

When symptoms of pulmonary fibrosis caused by radiation damage, the ensuing form of fibrosis is characterized as radiation induced pulmonary fibrosis (RIPF). It is a long-term and chronic side effect of healthy tissues receiving IR and can result from thoracic RT or any form of external beam RT which involves the deposition of IR into lung tissues [2]. The condition usually develops 6 months after the completion of treatment and can take anywhere between 6 to 18 after treatment to reach a stable state wherein the RIPF no longer grows or regresses [2], but there are cases where RIPF can become progressive. RIPF is preceded by a phase of acute inflammation caused by the immediate cellular apoptosis which occurs due to RT. However, it is uncertain whether this acute phase actually contributes to RIPF as there are many studies which demonstrate that acute inflammation does not correlate with RIPF severity or appearance [16, 17]. The contemporary evidence indicates that the severity of RIPF is largely proportional to the amount of radiation received per volume of healthy tissue [3]. Hence, outcomes of RIPF are maintained by keeping healthy tissue exposure to a minimum or, in cases where a therapeutic dose makes minimum exposure impossible, the protocol would be to maintain doses below empirically determined thresholds of dose per volume. While there are specific thresholds for maximum doses, these values are not consistent given the gradual and delayed response of RIPF, and the decision to exceed dose per volume recommendations as well as incurring acceptable levels of risks for adverse events are made based on clinical need and primary disease control, in the

case of NSCLC [18]. Currently, the accepted α/β ratio is 3.5Gy and recommendation suggest to maintain the volume of the lung receiving 20Gy (V20) to below 30-35% and limit the mean lung dose (MLD) to below 20 to 23Gy [18]. Again, reducing healthy tissue exposure will often require reduction of prescribed doses which will limit the amount of radiation applied to the target volume and thus limits the efficacy of RT. The avoidance of RIPF in clinical settings is due to RIPF's permanency, irreversibility and, in certain cases, progressivity [19]. In fact, RIPF is the most common reason for reducing treatment intensity or the abandonment of treatment [20].

RIPF Pathophysiology

On the cellular level, IR causes progressive damage to the lungs through triggering a multitude of cellular and molecular events that interfere with normal mechanisms of lung tissue repair. After lung irradiation, a majority of damage comes from the indirect production of radical oxygen and nitrogen species due to the ionization of oxygen or nitrogen compounds that naturally exist in the body [3, 21]. These radical and highly reactive species ultimately damage local deoxyribonucleic acids (DNA), lipids and proteins [3, 22] through the disruption of their molecular structure, mostly in the form of oxidation damage [3, 21]. Damage to lipids and proteins can cause arrest or disruption of certain specific metabolic enzymes, metabolic pathways and basal enzymatic activities, but the effects are minimal. It is the damage to DNA which results in the greatest effect. DNA damage disturbs DNA metabolism, triggering cascading failures of signaling pathways and failure of cell function which leads to transient or permanent cell-cycle arrest or apoptotic cell death [23]. The cell death and permanent cell cycle arrest often trigger the release of cytokines which leads to a loco-regional inflammatory reaction. This ultimately brings about the recruitment of inflammatory cells such as neutrophils, macrophages and lymphocytes, and culminates in the recruitment of fibroblasts, which proliferate and transform into myofibroblasts. In combination with the environmental growth factors and cytokines

released by the inflammatory agents, such as TGF-β, and damaged cells in the area, the myofibroblasts begin a process of extracellular matrix remodeling and deposition of large quantities of Extra-Cellular Matrix (ECM) proteins and collagen, specifically of the type-I and type-III variety [2, 15-17]. This process is roughly outlined in Figure 1.1.4.

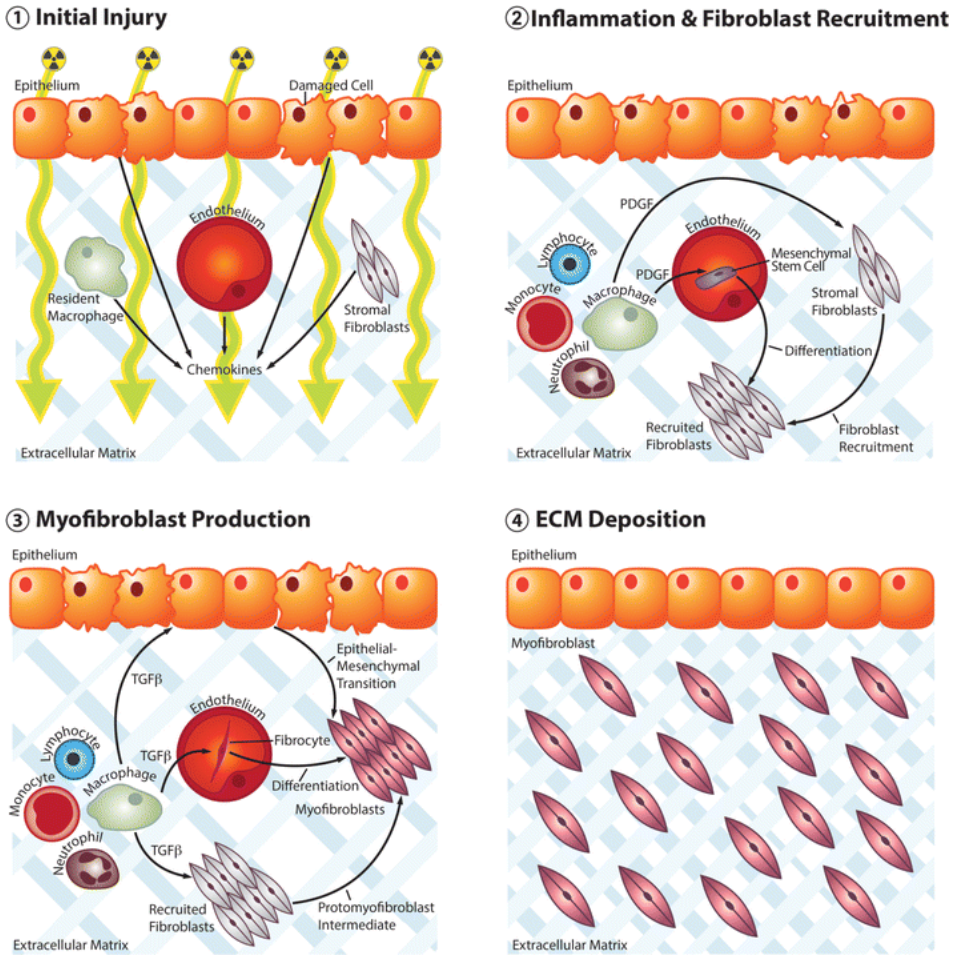

Figure 1.1.4 - Image and description taken from ref. [2]. Schematic depicting four broad stages in the pathogenesis of RIF. (1) IR damages cells in the exposed field and leads to the production of proinflammatory cytokines. (2) Neutrophils, lymphocytes, and monocytes arrive at the site of injury while resultant M2 macrophages produce PDGF, leading to recruitment of stromal fibroblasts as well as differentiation of circulating mesenchymal stem cells. (3) Subsequent TGF-β production by M2 macrophages promotes the development of myofibroblasts from recruited stromal fibroblasts through a protomyofibroblast intermediate as well as through epithelial–mesenchymal transition and differentiation of circulating fibrocytes. (4) Over time, myofibroblast proliferation along with excess

deposition and decreased degradation of extracellular matrix leads to fibrosis with reduced vascularity and a paucity of cells.

In the lung, the endothelial and epithelial cell population sustain the greatest damage after irradiation [24], through the radical induced cell death mechanisms mentioned above. Specifically, IR induces indirect production of free radical species and the subsequent disruption of DNA metabolism causes apoptosis of type-I and type-II pneumocytes, the two main cell types that constitute the alveolar epithelium [25]. Type-I pneumocyte is a complex differentiated cell lineage that carries out and optimizes the conditions for gas exchange in the alveolus and synthesizes, stores and releases pulmonary surfactant into the alveoli [25, 26]. Whereas, the pneumocyte type-II acts as a progenitor cell of the alveolar compartment (Figure 1.1.5). Type-II cells responds to damage of the labile type-I cell by dividing and differentiating to replace both type-I and type-II cells. After irradiation, it is thought that type-I cells are denuded, and the proliferation of type-II pneumocytes is stimulated. But it has been reported that irradiation causes senescence of endogenous type-II pneumocytes, likely resulting in the creation of a defective repair mechanism, which can only replace the functional type-I pneumocytes with non-functional fibrotic tissue [15, 27]. This inability to replace the lost functional type-I and type-II pneumocytes is coupled with the loss of and inability to regenerate vessel and interstitial integrity. This increases the recruitment of a variety of inflammatory cells to the site of injury, through secretion of growth factors and proteases, eliciting repair processes and the degradation of extracellular matrix to allow for removal of dead cells [15, 27, 28]. Sustained tissue and cellular damage in this state causes a cascade of events leading to chronic tissue inflammation, triggering long-term secretion of cytokines, growth factors and immune responses in the lungs [2, 15-17], in combination with the recruited fibroblasts and matured myofibroblasts. This initiates a more permanent restructuring of the extracellular matrix, promoting the production of type-I collagen and causing the deposition of collagenous and fibrous scar materials that are hallmarks of pulmonary

fibrosis. This sequence of cell death, tissue damage and tissue restructuring, is what ultimately results in the replacement of lung functional tissue with collagen, causing the RIPF characteristics of thickening, stiffening of the interstitial structures and, most importantly, loss of pulmonary function [2, 16, 17, 27]. This phase of collagen deposition continues for 6 to 18 months, where slight restructuring of the extracellular matrix occurs before the fibrosis permanently stabilizes. There are also instances where RIPF becomes progressive and the condition worsens, never reaching a stabilized state [2].

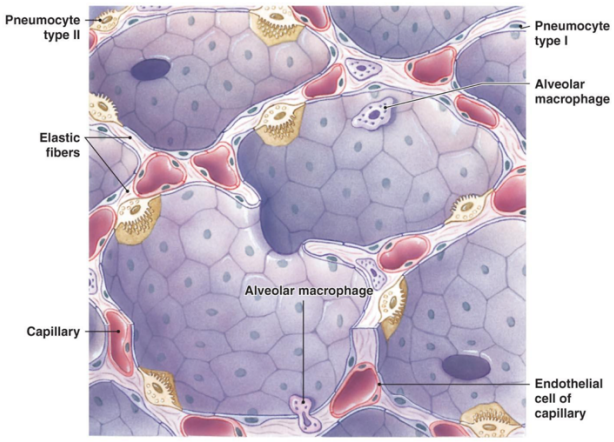

Figure 1.1.5 – Image taken from ref. [29]. Cellular structure of the alveolar compartment including the presence of type-I and type-II pneumocytes. The yellow substance which surrounds the capillary and is between layers of type-I cells is the basement membrane containing miscellaneous structural proteins.

Histopathological Assessment of RIPF

The main method for a histopathological identification of RIPF involves the appraisal of: 1) pulmonary and interstitial structures integrity and organization or lack thereof, 2) deposition of fibrous connective tissues such as collagen and 3) severity of immune response [30, 31]. The sample, often acquired through biopsy, must be prepared using staining methods allowing for the visualization of all three of these elements, with specific focus on collagen. The most popular methods to specifically

visualize and appraise fibrosis are staining with Masson's Trichrome, Van Gieson's Stain and/or Sirius Red (Figure 1.1.6). While all three methods impart a different quality to the stained sample, highlighting different cellular structures through the use of different colors. The function of the three stains are similar in that they allow the collagen to be differentiated from surrounding cells and tissues, whether through contrast from surrounding tissues in color or texture and allows for the visualization of tissues structures and their integrity or lack thereof. Additionally, the use of Hematoxylin & Eosin (H&E) is a general staining technique which can allow for fibrosis visualization but is not specific in highlighting the elements of fibrosis and will give an impression of the general structures within the region.

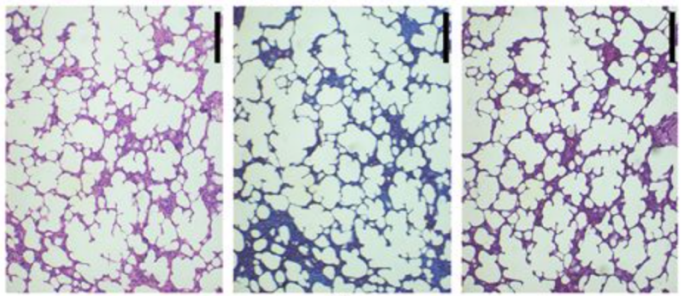

Figure 1.1.6 – Image adapted from [32]. Image depicting the staining of an alveolar field with H&E (left), Masson's Trichrome (middle) and Sirius Red (right). Gieson's stain is not included

Currently the most commonly utilized method of staining is Masson's Trichrome, its use of opposing colors, blue and red, makes visual identification of collagen easier. In Masson's Trichrome, the fibers of collagen which comprises the fibrosis are stained an easily identifiable bright blue (Figure 1.1.7). This quality is opposite to Sirius Red and H&E protocols which stain tissue elements in relatively similar colors, such as red, orange and yellow (Sirius Red) and different shades of pink (H&E).

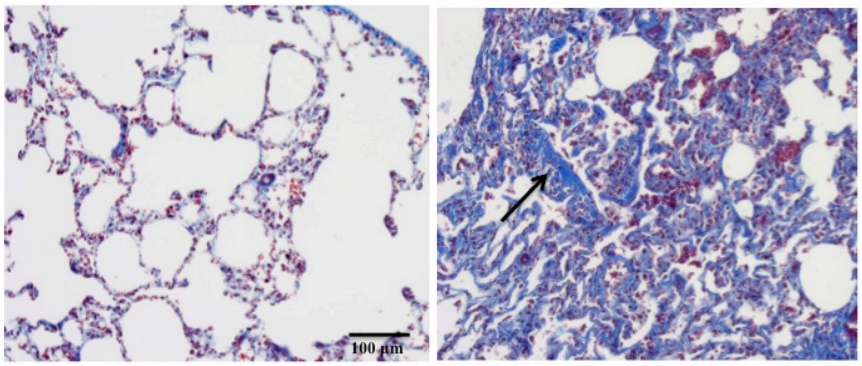

Figure 1.1.7 – Images we produced of Masson's Trichrome stained alveolar fields. Note the appearance of the bright blue, corresponding to collagen, being easily distinguishable from other elements such as epithelial cells, immune cells and red blood cells.

Clinical Presentation and Assessment of RIPF

In the clinic, patients usually present with symptoms and imaged findings of RIPF 6 to 12 months post-irradiation [25]. The main method of RIPF identification is through CT imaging, where RIPF appears as patchy opacities (Figure 1.1.8). The use of radiography and magnetic resonance imaging (MRI) are also appropriate and useful imaging techniques. Often times, RIPF in clinical imaging is one of a multitude of adverse events, occurring along-side pneumonitis, pulmonary infections, primary disease recurrence in the case of NSCLC, edema, atelectasis, chronic obstructive pulmonary disease (COPD), partial or complete pneumothorax and other inflammatory diseases of the lung which can be caused by RT, existing comorbidities or concomitant chemotherapies. The extent and number of these adverse events is often related to the treatment of a primary disease such as NSCLC and the presence of comorbidities in the patient. Many of these intersecting diseases causes similar opacities that can be confused with RIPF, but there are qualities to RIPF which makes it visually distinct from other comorbidities (Figure 1.1.9). The mentioned opacities will fluctuate in size such as that opacities within 6 months of treatment are usually events of pneumonitis or atelectasis and obstructive inflammation due to the primary disease. At this initial period of fluctuations, if RIPF does exist, its

size is likely to be small, diminished or diffused, being indistinguishable from the temporary inflammatory events. Beyond 12 to 24 months post-treatment, most instances of pulmonary inflammation would have subsided and growth or reduction of RIPF has ceased and reached a state of permanence [27, 33, 34]. It is at 6 to 12 months post-treatment, when physicians can better identify and distinguish instances of RIPF from the other accompanying inflammatory sequela.

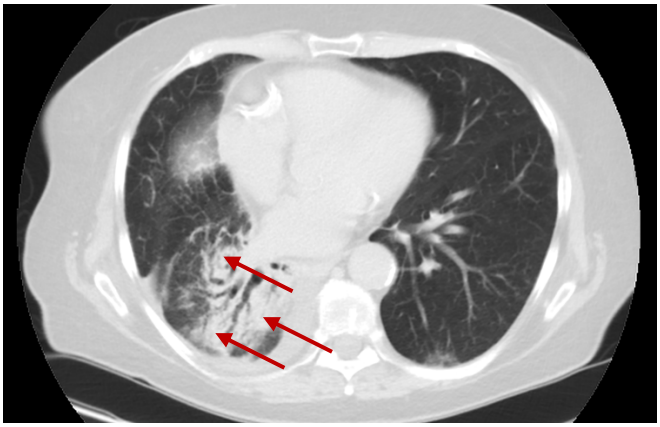

Figure 1.1.8 – Fibrosis imaged on a follow-up patient CT image (red arrows). Fibrosis often occurs in discrete volumes with specific textures. Imaging taken from our prospective patient study with reading provided by Dr. Alexandre Semionov.

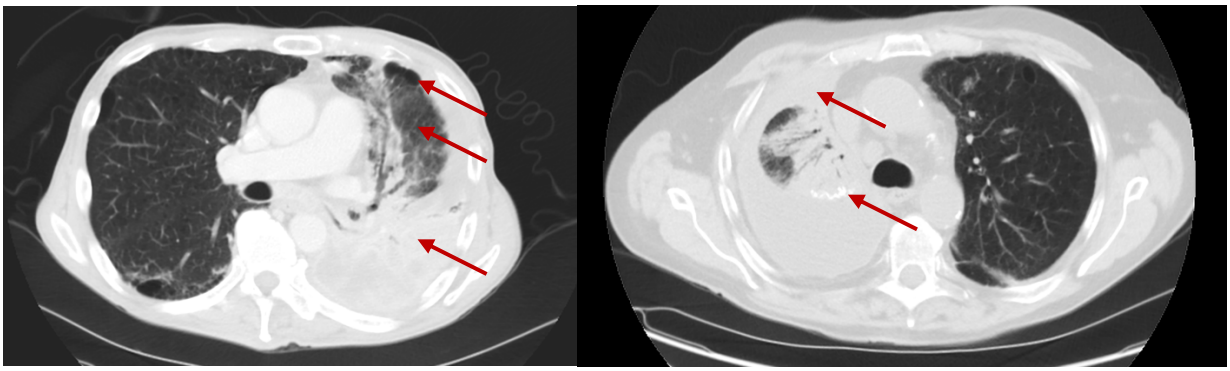

Figure 1.1.9. – Imaged instances of potential comorbidities (red arrows) that occur along with RIPF. In the left image, instances of cavitation (top), ground glass opacities indicative of pneumonitis (middle) and what is likely a pneumothorax or edema (bottom). On the right there is likely a pneumothorax or edema event (top) coupled with calcification (bottom). Imaging taken from our prospective patient study with reading provided by Dr. Alexandre Semionov.

Symptomatically, identifying RIPF is more challenging. Clinical testing involving the assessment of pulmonary function, such as forced expiratory volume (FEV) or peak expiratory flow (PEF) can be used to identify deficits in breathing ability or symptoms of dyspnea, trouble breathing or chest pains [18, 25, 27] which could accompany RIPF. However, results from these functional tests are often unclear due to NSCLC patients having poor baseline function and, coinciding with the treatment and regression of their primary disease, patients will often experience better functional abilities despite RIPF development and progression. Along the same lines, it is also problematic when attempting to identify instances of RIPF through symptomology. In cases of patient self-reports, patients often are asymptomatic and do not report breathing troubles during follow-up consultations post-treatment. This is due to the improved quality of life and lung function due to regression of the primary disease overcoming the detriment brought about by RIPF symptoms [18, 35, 36]. This difficulty is compounded by the fact that inconsistencies between and diverse subjective interpretations of the RIPF scoring systems' criteria lead to irreproducible RIPF assessments [35]. The development and presentation with regards to RIPF can vary widely among patients, with some patients exhibiting quick progression towards fatal outcomes while other patients presenting asymptomatically [20].

Treatment for RIPF

Currently, there is a lack of FDA approved curative treatments which tackles the underlaying molecular processes of RIPF [17], mostly due to the complexity of the mechanisms leading to RIPF [18]. Current therapies are designed just to reduce symptoms of RIPF, as well as stall progressive instances of the disease through reducing inflammation or altering the inflammatory response but these therapies are generally ineffective or inconsistent in their efficacy. For example, anti-inflammatory therapy has been used extensively to treat radiation injury. Corticosteroids and non-steroidal anti-inflammatory drugs are of value in the pre-fibrotic phase and in reducing the acute

inflammation associated with fibrosis. But, signs and symptoms may recur after the cessation of corticosteroid therapy, and prophylactic administration of corticosteroids does not always appear to be beneficial [17, 37] and has also been linked to increased likelihood of cancer metastasis. Other therapies have also been tested in interventional clinical studies, such as vascular therapy with pentoxifylline or hyperbaric oxygen; treatment with antioxidants like superoxide dismutase, vitamin E (alpha-tocopherol), and with a pentoxifylline and vitamin E combination [2, 21, 27]. But these therapies only can target a few of the elements involved in RIPF development and progression and, as such, the benefits to patients are few and too varied to be of therapeutic value [37, 38].

The use of stem cells as an alternative therapy, after major functional tissue loss, has arisen as a possible solution. The use of mesenchymal stem cells (MSCs) as an alternative treatment for cardiac [39], parotid gland damage [40] and fibrosing diseases [41] demonstrates the possible impact of MSCs in reducing functional-loss/fibrosing diseases of the lung. The main proposed mechanisms through which MSCs carry out their reparative effects, following tissue damage, include the capacity of homing to sites of injury due to local release of chemokines [42, 43], the ability to release anti-inflammatory soluble factors, and immunomodulatory properties [41, 44]. These characteristics appear capable of countering or reducing the chronic inflammation which leads to the development of RIPF. In addition, MSCs, being multipotent cells, have potential to differentiate into a variety of cell types [45] giving MSCs potential regenerative properties, through engraftment, differentiation and replenishment of local cell populations, although, the partial engraftment and retention [46, 47] has not been shown to correlate with functional improvement [48]. The immunomodulatory roles that therapeutic MSCs play, through the increased expression of anti-inflammatory cytokines have been demonstrated in acute kidney [43], liver [49], and lung [50] injury animal models. These beneficial paracrine effects have also

been reported in animal models of myocardial infarction [51], stroke [52], sepsis [53], and chemical [54] and physical damage [55].

In specifically treating RIPF, the literature reports that the main method of action is through replacing lost pneumocytes by the differentiation from the MSCs [56] and taking advantage of the MSC's immunomodulatory properties [57]. There have been reports of MSC differentiation potential after radiation induced lung damage in an *in vivo* mouse model utilizing 2×10^5 MSCs intravenously injected via the tail vein [24]. The study proposed that the time frame for MSC administration, post-irradiation, is important in determining which type of cells MSCs will differentiate into, finding that the 15% of MSCs administrated soon after irradiation will differentiate into pneumocytes type-II, possibly contributing to replacing the loss of functional pneumocytes due to radiation damage [24]. Other studies have shown and suggested that therapeutic effects come about through MSC engraftment, differentiation and replacement in addition to some level of MSC-produced oxidative stress modulation [58]. With local administration of MSCs shown to improve its retention and beneficial effects on injured organs [59-61] including the lungs [62, 63]. Promising results have shown that the reduction of fibrosis, utilizing MSCs, is reproducible in other models of injury besides radiation. For instance, MSCs reduce bleomycin induced pulmonary fibrosis when administered via the tail vein [58, 64], and intratracheally [65]. And beyond just the administration of allogeneic MSCs, granulocyte-macrophage colony stimulating factor (GM-CSF) can be used to induce the mobilization of endogenous MSCs to sites of injury. The use of GM-CSF has been reported to help repair injured myocardium [66], lung [67] and pulmonary injury due to bacterial infection [68].

1.2 – Qualitative Appraisal of RIPF

Qualitative RIPF appraisals are any kind of scoring of RIPF carried out visually by a professional. Depending on whether the RIPF event is captured in the form of a clinical diagnostic image, such as CT, MRI or radiography, or a biopsy, a clinician or a pathologist, respectively, will be called upon to make the assessment as to the extent and severity of RIPF. However, in both of these circumstances, the efforts applied are expended to determine if a patient requires the necessary attention and intervention. Specifically, in the case of NSCLC patients who have undergone treatment, the identification and diagnosis of RIPF is to communicate the existence of a toxicity that is to be observed for and treated appropriately if encountered. In general, the status of a patient's RIPF is taken into account only in circumstances where the patient's overall well-being or potential well-being will be impacted. As such, the ontology for, categories of severity given to and language used to describe RIPF events is diverse, inconsistent and difficult to replicate [18, 35] as the descriptions are often unique and circumstantial.

This inconsistency and non-reproducibility are likely exacerbated further by two factors: 1) The subjectivity of the qualitative appraisals and 2) the clinical motivations for RIPF assessment. The first factor of subjectivity is innate to any activity that requires the opinions and interpretations of a sole specialist or multiple specialists. This is especially problematic when comparing appraisals performed by multiple physicians. Factors such as experience, training and aptitude make a difference in terms of image features that physicians are drawn to and place emphasis upon [69]. Even if we control for the radical differences that comes from physicians of very different levels of experience and training, even for similarly trained and experienced physicians, there can still be different interpretations arising from the same set of evidence. Personal dispositions, which differ from individual to individual, can also lead to differences in how imaging evidence is interpreted [69]. Alternatively, the same physician

can also interpret evidence differently. The additional experience and the different attitudes that a physician has at two different points in their career or even at two different points of the week can lead to different interpretations of the same set of evidence. While this difference seems to highlight an innate weakness of physician diagnoses, the more appropriate interpretation, in regard to RIPF specifically, is that the criteria appraising RIPF is flawed and relies too heavily on circumstantial construction of disease description. The criteria for RIPF needs to be formalized into a heuristic which simplifies the diagnostic process and removes the need for subjective appraisals that a physician needs to make [35].

In relation to the lack of formalization, there is the question of motivation for diagnosis. In the current form, criteria for RIPF diagnosis is adequate and serves the purpose of diagnosis for the sake of providing evidence for action on a case-by-case basis. Currently, RIPF scoring is a metric predicated on, in the broadest sense, quality of life and formulated for the goal of identifying the need for intervention for a single patient as opposed to generalized disease description. This means that the process is often satisfied with merely identifying the presence or absence of a certain disease, with minimal identification of severity when necessary. And given the circumstances, there is most likely inertia in formalizing heuristics driven by the measurement of biomarkers to formulate exacting details of a particular RIPF event as doing so does immediately prove to yield improved clinical discourses or better clinical outcomes.

There are attempts at creating criteria by which to standardize physician appraisals and curtail elements of subjectivity and the case-by-case type of approach. These criteria take the form of scales which delineate discrete severities of a single disease event. They have been applied to limited efficacy [35] in generating usable outcomes but they are nevertheless useful in establishing a standardized language from which to talk of outcomes.

Grading Scales for RIPF Assessment

In identifying RIPF, there are currently many criteria or grading scales that are implemented and designed to allow for a high degree of consistency across inter- and intra-observer grading. Most of these are designed to be more rigorous through establish a levels of observation detail that stresses specific qualities which falls under each degree of severity.

For histology, there are several main criteria for scoring instances of RIPF. The two most popular methods are the Ashcroft and Wagner. The Wagner is a generalized grading scale that allows for the qualitative assessment of nonmalignant respiratory diseases [70]. The scale is not widely used and was modified at the turn of the 2000s in order to allow for a better differentiation between fibrosis grades [70]. Alternatively, there is the Ashcroft scale which was designed as a generalized grading scale for assessing a variety of pulmonary variables [31]. The details and criteria of this scale was modified more recently in order to achieve better performance [30] (Figure 1.2.1). Between these two grading scales, there are also a large variety designed with details and criteria for locating specific features in histological samples. Most if not all of these scales are used circumstantially depending on the disease in question and what qualities relating to the disease is of interest to be graded and assessed.

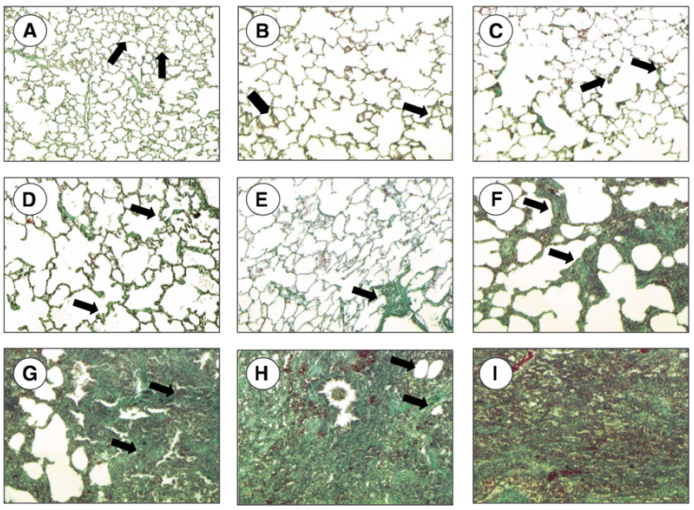

Grade of Fibrosis	Sample Photograph	Modified Scale
0	Figure 1A	**Alveolar septa**: No fibrotic burden at the most flimsy small fibers in some alveolar walls **Lung structure**: Normal lung
1	Figure 1B	**Alveolar septa**: Isolated gentle fibrotic changes (septum ≤3× thicker than normal) **Lung structure**: Alveoli partly enlarged and rarefied, but no fibrotic masses present
2	Figure 1C	**Alveolar septa**: Clearly fibrotic changes (septum >3× thicker than normal) with knot-like formation but not connected to each other **Lung structure**: Alveoli partly enlarged and rarefied, but no fibrotic masses
3	Figure 1D	**Alveolar septa**: Contiguous fibrotic walls (septum >3× thicker than normal) predominantly in whole microscopic field **Lung structure**: Alveoli partly enlarged and rarefied, but no fibrotic masses
4	Figure 1E	**Alveolar septa**: Variable **Lung structure**: Single fibrotic masses (<10% of microscopic field)
5	Figure 1F	**Alveolar septa**: Variable **Lung structure**: Confluent fibrotic masses (>10% and ≤50% of microscopic field). Lung structure severely damaged but still preserved
6	Figure 1G	**Alveolar septa**: Variable, mostly not existent **Lung structure**: Large contiguous fibrotic masses (>50% of microscopic field). Lung architecture mostly not preserved
7	Figure 1H	**Alveolar septa**: Non-existent **Lung structure**: Alveoli nearly obliterated with fibrous masses but still up to five air bubbles
8	Figure 1I	**Alveolar septa**: Non-existent **Lung structure**: Microscopic field with complete obliteration with fibrotic masses

Figure 1.2.1 (left) & Table 1.2.1 (right) – Modified Ashcroft scale taken from [30]. Alveolar fields (left) corresponding with the grades attributed in the modified grading scale (right). Higher grades involve greater destruction of regular interstitial and alveolar structures in addition to greater deposition of collagenous fibers. Although at the highest grades, grading largely depends on structural destruction.

In the clinical realm, there is a large selection of grading systems that are also circumstantial in their utility. Among them, the Common Terminology for Adverse Events (CTCAE) is the most commonly used. These scales provide a reference as to what constitutes a given severity for an adverse event. In the case of pulmonary fibrosis in the most recent version of the CTCAE, version 5.0, pulmonary fibrosis is determined based on a combination of symptomatology and imaging evidence [71] (Figure 1.2.2). With increasing severe symptomatology and larger radiographic findings proportional to grade. In general, the CTCAE is constructed to assess the quality, or lack thereof, associated with a given adverse event. Hence, death, due to the disease being observed, constitutes a grade 5. Correspondingly, more severe impairment due to the appraised disease results in a higher grade.

Respiratory, thoracic and mediastinal disorders					
CTCAE Term	**Grade 1**	**Grade 2**	**Grade 3**	**Grade 4**	**Grade 5**
Pulmonary fibrosis	Radiologic pulmonary fibrosis <25% of lung volume associated with hypoxia	Evidence of pulmonary hypertension; radiographic pulmonary fibrosis 25 - 50% associated with hypoxia	Severe hypoxia; evidence of right-sided heart failure; radiographic pulmonary fibrosis >50 - 75%	Life-threatening consequences (e.g., hemodynamic/pulmonary complications); intubation with ventilatory support indicated; radiographic pulmonary fibrosis >75% with severe honeycombing	Death
Definition: A disorder characterized by the replacement of the lung tissue by connective tissue, leading to progressive dyspnea, respiratory failure or right heart failure. **Navigational Note:** -					

Table 1.2.2 – Image of the CTCAE extracted from [71]. Note the necessity for radiological evidence and symptomology in order to determine disease grade. With increasingly severe symptomology and greater radiographic findings correlating with a higher score.

Another widely used scale is the late effects in normal tissue-subjective objective management analysis (LENT-SOMA), shared by the Radiation Therapy Oncology Group (RTOG) and the European Organization for Research and Treatment of Cancer (EORTC) [72]. However, its main function is not to specifically identify the severity of an adverse reaction like RIPF. In fact, it is used as a general means to evaluate the condition and function of the lung. As such, between the use of the CTCAE and LENT-SOMA in the clinic, there has been disagreement leading to the possibility of inconsistent scoring and nonreplicable assessment of RIPF [35].

1.3 – Quantitative Analysis of RIPF

While qualitative assessments are effective in identifying disease and helping direct clinical decisions, they lack the necessary precision to be effectively used in long-term tracking of symptomologies, due to non-replicability and subjectivity. In addition, qualitative assessments required large time commitments of more than one professional observer. The professional in question were typically physicians with limited free time. This means that these qualitative assessments are too difficult to be used in research endeavors as descriptive biomarker. Alternatively, providing long term RIPF disease tracking for patients also proves to be very difficult given the amount of time and effort required to assess patients. Hence, there is a movement [73-75] towards utilizing objective biomarkers derived

directly from physical or diagnostic evidence, without the need for or to, at the very least, limit subjective interpretation of the evidence.

For RIPF, one of the most important and dependable diagnostic elements which provide evidence for the presence/absence of RIPF and the severity of RIPF is diagnostic imaging. To this end there has been development of novel techniques for categorizing and scoring fibrosis that limits the need for subjective interpretation of these images and instead utilizes objective metrics that can be extracted from these images.

Colorimetric Analysis

In images where the presence of specific colors and quantities of these colors highlight phenomenon of interest, an analysis of color distribution or of the quality of the color itself can constitute an informative quantification. This is most relevant for studies and techniques which involve histology or immunofluorescence, where the chemical dyes or fluorescents highlight important regions in a sample with a color that allows for high contrast and visual identification. In techniques, such as immunofluorescence, where concentration of a particular substrate is proportional to fluorescence intensity, quantification of fluorescence intensity can lead to identification of substrate concentrations in an unknown or experimental sample through the use of a standard curve.

Alternatively, techniques which quantify attributes relating to color in an image can be made automatic and more precise, something that traditional qualitative appraisals cannot achieve. The inclusion of more specific criteria, such as the delineation and quantification of areas according to a specific hue, saturation and brightness value can allow for the acquisition of very specific data which human observers cannot differentiate. This technique, of color separation and area of color quantification, is

applied to great efficacy when utilized with full slide images of histological samples to capture the exact region of effect for a disease like fibrosis (Figure 1.3.1).

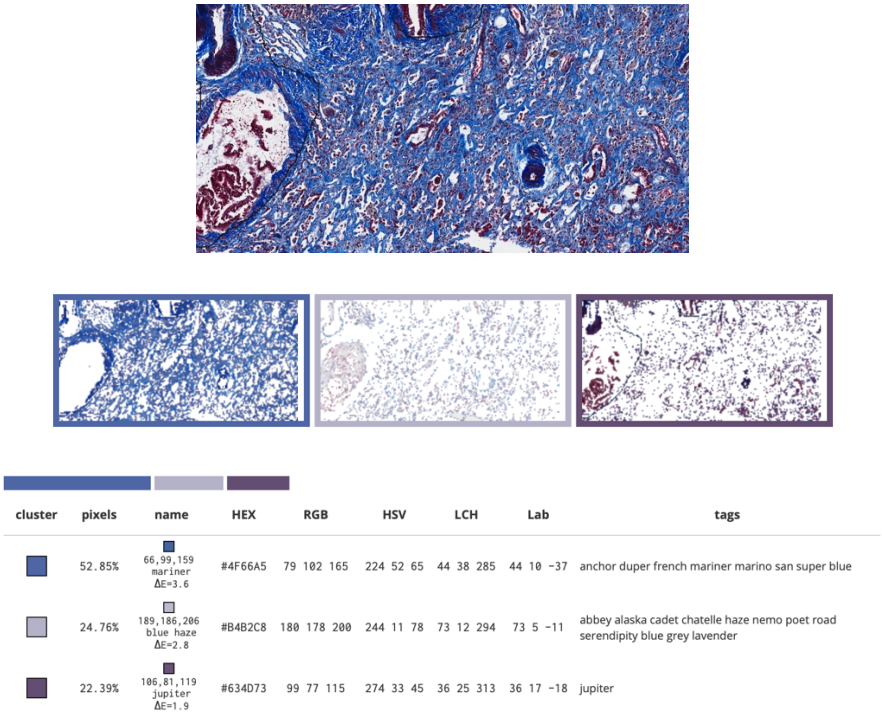

cluster	pixels	name	HEX	RGB	HSV	LCH	Lab	tags
	52.85%	66,99,159 mariner ΔE=3.6	#4F66A5	79 102 165	224 52 65	44 38 285	44 10 -37	anchor duper french mariner marino san super blue
	24.76%	189,186,206 blue haze ΔE=2.8	#B4B2C8	180 178 200	244 11 78	73 12 294	73 5 -11	abbey alaska cadet chatelle haze nemo poet road serendipity blue grey lavender
	22.39%	106,81,119 jupiter ΔE=1.9	#634D73	99 77 115	274 33 45	36 25 313	36 17 -18	jupiter

Figure 1.3.1 - Image analysis extracted completed using software from ref. [76]. An example of a quantitative analysis for color in histological samples. The software is able to segregate (middle three images) and calculate proportional area as well as identify the quality of the colors (bottom chart) for the three major colors which appear in the raw sample image (top image).

Radio-densities

One of the most applicable methods of quantifying RIPF is through the use of CT radiodensities. In the context of biological and diagnostic imaging, x-ray passage through a material is inversely proportional to the density of the material. Given constant thickness, more dense materials also tend to me more radio-dense (Figure 1.3.2). In this case, every element within a CT image, which is a combination of x-ray emission scans combined into a 3D volume, has a measure of radiodensity

represented by a Hounsfield Unit value. This characteristic allows for the opportunity to quantify radio-densities in any given region [77].

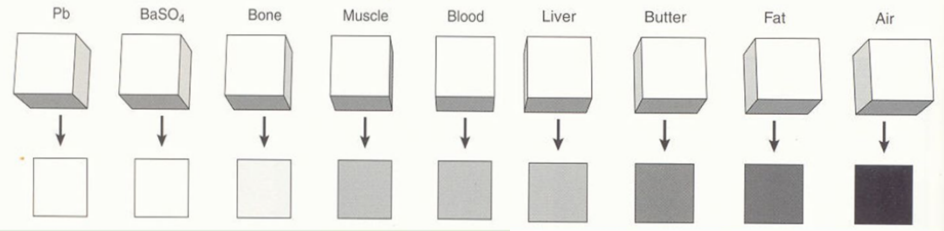

Figure 1.3.2 – Image taken from ref. [78]. Image depicting radiodensities of common materials. Fibrosis falls between muscle, blood and liver depending on how diffuse the fibrosis in a given region is. The less dense the accumulation of fibrosis, or ECM proteins are in a region, the less radio-dense that region will be as well.

In quantifying RIPF, deposited type-I, type-III collagen and other miscellaneous ECM proteins is of greater radio-density than surrounding structures, which are predominantly air (Figure 1.3.3). In a typical CT image of healthy lungs, the vast majority of the lung volume has a radio-density from -800 to -1000 HU [75, 79]. This is in contrast to fibrosis which occupies a radio-density range of -300 HU or greater depending on the density of accumulated fibrosis [75].

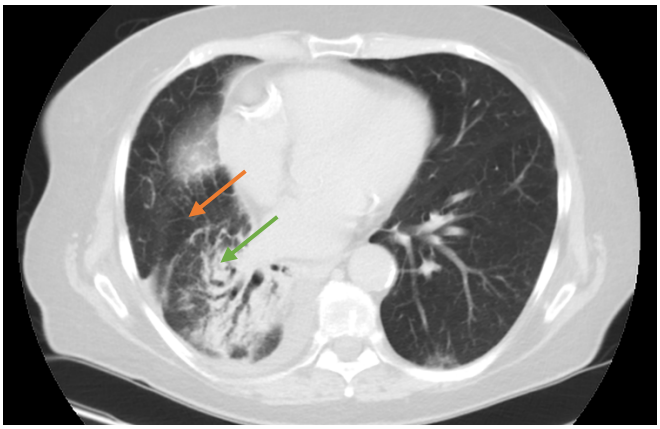

Figure 1.3.3 – Fibrosis imaged on a follow-up patient CT image (green arrow). The greater radio-density of the fibrotic region can be distinguished from the regular pulmonary structure densities (orange arrow). Image reading performed by Dr. Alexandre Semionov for the pilot study.

Quantification of fibrosis typically involves establishing thresholds for what are believed to be fibrotic densities, using clinical contours of structures, and then generate a value of fibrotic damage in proportion to the entire volume of the lung. Alternatively, instead of utilizing proportions in relation to the volume of the whole lung, scoring could also take the form of average or median radio-densities in any given volume of the lung. An alternative to whole lung analysis is a region of interest (ROI) analysis, where proportions, averages or medians are taken from within limited specific regions, whether regular or random, in the lung rather than the entire lung.

In terms of quantifying radio-densities, one of the greatest challenges is being able to establish baselines for comparisons. Even without the addition of opacities due to the involvement of RT or treatments, the lung anatomy will undergo changes over time. Even on the scale of minutes, breathing or the movement of the heart can cause the lung volume to change. This poses a problem for analysis of whole lung volumes. To some degree, it also affects ROI analysis, but is less impactful given that the ROIs are only partial lung volumes and are less affected by changes to the entire volume. In context of RT, the lung anatomy experiences more changes that can make whole lung analysis more difficult. The presence of other toxicities due to treatment or comorbidities such as atelectasis, chronic obstructive pulmonary disease (COPD), pneumonitis or edema can make interpreting baseline imaging difficult as it will be difficult to establish the baseline and what is: 1) the underlying RIPF instance, 2) the expected volume of the lung, and 3) the expected condition of the lung. Over multiple time-points with the fluctuations in severity of the toxicities, comorbidities and primary disease, due to treatment, this masking of RIPF by comorbidities or anatomical changes becomes more problematic and would make differentiating RIPF more difficult. In these cases, a specialized tool or technique would be required to control for these factors in the imaging. Of course, ROI analysis can be tailored to specifically avoid instances of comorbidities, toxicities or fluctuating primary disease but

there is no guarantee that the regions chosen will be adequate or representative of the entire lung condition. Currently, there is no clear answer as to which is better, and the type of analysis is chosen and performed circumstantially.

The quantification of radiodensities has been used in animal models as well as retrospective patient studies. There are currently no distinctions between the analysis for animals and humans, as both organisms can be scored for fibrosis using this technique. However, the higher relative resolution of human CT imaging, due to the dimension of the organism, makes this method more viable as the greater number of voxels present in a CT volume allows for greater statistical power.

Image Registration

Image registration is a mathematical technique whereby one image, or a set of vectors, is transformed to fit the shape of another image, or another set of vectors. This mathematical comparison itself, between the two images, can generate values which indicate the magnitude of difference and distortion which has occurred between the two images (Figure 1.3.4). Through the utilization of these distortion values, image registration also opens up the possibility for aligning two images despite them being different or having been altered. The registration transformation applied in order to align the two images can be one of rigid or deformable registration [80]. Rigid registration involves simple transformations such as translations or rotations of one image to align it with another. Whereas deformable registration uses a non-uniform mapping between the images and corrects for small discrepancies in a follow-up image (Figure 1.3.4).

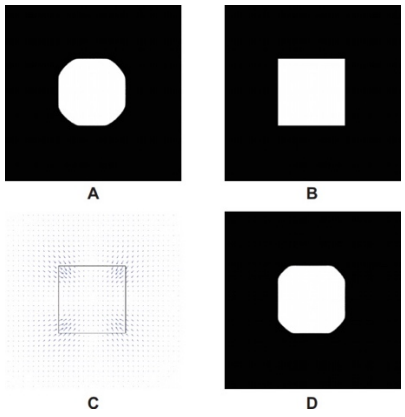

Figure 1.3.4 – Image taken from ref. [80]. A simple example of deformable registration of shape B (deemed the moving image) onto shape A (deemed the fix image). C depicts the change in spacial vectors of shape B in order to align B to A. D is ultimately the product of the deformable transformations applied. Note that it will not always be the case that the transformation applied will create a perfect alignment. The strength of a transformation is adjustable depending on utility and setup.

The main implication of image registration in the detection of RIPF is that it offers the means by which a follow-up image, acquired for diagnostic purposes following treatment, can be compared to the baseline image. Assuming that RIPF developed as a result of treatment for a primary disease, such as NSCLC, analysis can be conducted to compare the follow-up image, depicting an instance of RIPF, with the baseline image, depicting the absence of RIPF. The use of specifically deformable image registration also allows for the compensation and correction of changes in the images which includes, but are not limited to, anatomical changes caused by comorbidities or primary disease and changes in anatomical volumes due to physical movement, breathing or heart palpitations. The ability to generate values which correspond to the degree of change between two images allows for an analysis of structural deformation which occurred due to RIPF. For example, the changes in size of certain pulmonary lobes or segments, the change in shape of the bronchial tree [73] and even the movement of primary disease or region of RIPF can all be quantified and analyzed. This provides a possible means of objectively, precisely and reproducibly capture changes in 3D delineated structures in

imaging. Alternatively, the use of these deformation values can then be applied to follow-up images to transfer the same volumes or structure in a set of diagnostic images onto follow-up images. For example, PTVs that were clinically contoured by technicians or clinicians can be automatically mapped to a follow-up image despite the changes that may have occurred in the follow-up imaging due to anatomical alterations or motion. This technique offers the ability for quantitative methods to correct for circumstantial changes that physicians, or professional human observers, automatically perform due to experience.

1.4 - Thesis Objectives

The objectives of this thesis were the following:

- establish a method of quantifying RIPF that is objective, replicable and rigorous
- verify that such a data driven solution is feasible
- validate if radiodensity is an adequate metric for assessing RIPF
- validate if colorimetric based analysis is an adequate metric for assessing RIPF in histopathological samples
- comparing the proposed framework and method of analysis against the assessment capabilities of specialists in a clinically relevant utility

Scope of Project

RIPF is a specific toxicity experienced following thoracic RT. It delineates a discrete disease that occurs in the long-term and is generally a component of radiation induced lung damage. Current methods of RIPF identification have been inadequate in being able to specifically identify RIPF in NSCLC patients due to similarly appearing toxicities which occur due to RT for NSCLC as well as the subjectivity and case-by-case nature of current clinical practices for RIPF assessments. Current research within the domain of quantifying radiation induced damage have all been efforts to merely quantify, without attempts at applying quantification to generate usable clinical outcomes. The two studies included in this thesis will aim to establish and implement designed quantitative methods for assessing RIPF, in histology and in diagnostic CT imaging, in order to assess the effect of stem cell therapy using a RIPF rat model, and to assess the effect of RT treatment modalities on RIPF severity in NSCLC patients.

In order to enhance the precision of the quantitative method, the studies established and implemented a unique methodology of biomarker design whereby a quantity to be extracted is specifically tailored to exclude elements which can confound results. This is unique, as current literature emphasizes the use of many biomarkers versus the use of a few specifically designed ones, with the intention that the information introduced by more biomarkers will overcome inherent confounding factors. The methodology for quantification using a method of selective colorimetric analysis in histopathology samples from the rat model and using a selective radio-density measure in patient CT imaging was applied to a group of 25 rats and 86 patients respectively.

This study is prospective and is intended that subsequent investigations which utilize this method could do so without much modification to the current protocol. The purpose of this work is not to purely establish that quantitative methods are better than qualitative methods or that a specific quantitative method is better than another. Rather it is and attempt to apply design-based biomarkers to generate relevant and usable outcomes specifically relating to RIPF. The study is also an attempt at understanding how these quantitative methods will fair when compared to traditional specialist appraisals and whether the same results and conclusions can be drawn from them.

1.5 - Thesis Overview

The thesis is structured to present two publications within its contents as well as illustrate two concurrent studies that were conducted to validate the capabilities of a quantitative system of RIPF scoring. As such, Chapter 3 will be the first of the two manuscripts, detailing the validation of the quantitative analysis for histopathological identification and grading of RIPF in a rat model. Chapter 5 will be the second of the two manuscripts, detailing the validation of the automated quantification of RIPF in human patients through the comparison of RIPF outcomes with respect to treatment modalities. Chapter 6 and 7 will be the general discussion and conclusion of the thesis. In Chapter 7, I will present some directions for future development as well as proposals for possible applications.

§2 Preface for Manuscript #1

In chapter 3, we attempt to validate the efficacy of administered MSC in reducing the severity of RIPF and comparing the efficacy of different modes of MSC administration. Here, comparisons were made of RIPF scoring by a certified pathologist and scoring derived from quantifying fibrosis in histopathological imaging. We were able to verify that MSCs can prove to be of benefit and that the use of GM-CSF is the most affective of the different modes of administration. Furthermore, we validated that our model of an automated and quantitative method of scoring RIPF in histopathological imaging is feasible and shows potential. But currently lacks the important ability to assess structural changes due to RIPF.

§3 Stem cell administration effect on sub-regional response of radiation-induced pulmonary fibrosis in a rat model

Li Ming Wang[1,2,*], Sungmi Jung[3], Monica Serban[4], Sangkyu Lee[5], Krishinima Jeyaseelan[5], Avishek Chatterjee[5], Issam El Naqa[6], Jan Seuntjens[2,4], Norma Ybarra[1,2,4]

* To whom correspondence should be addressed: li.m.wang@mail.mcgill.ca
Phone: 1 (647) 867-4811

Keywords: Radiation induced pulmonary fibrosis (RIPF), Mesenchymal stem cells (MSCs), granulocyte-macrophage colony stimulating factor (GM-CSF)

Running title: Stem cell administration effect on sub-regional response of radiation-induced pulmonary fibrosis in a rat model

[1] Cancer Research Program, Research Institute of the McGill University Health Centre, 1001 Décarie Blvd, H4A 3J1, Montréal, Canada

[2] McGill University, 845 Sherbrooke St W, H3A 0G4, Montréal, Canada

[3] Royal Victoria Hospital, McGill University Healthcare Centre, 1001 Décarie Blvd, H4A 3J1, Montréal, Canada

[4] Medical Physics Unit, Cedars Cancer Centre, McGill University Healthcare Centre, 1001 Décarie Blvd, H4A 3J1, Montréal, Canada

[5] Memorial Sloan Kettering Cancer Centre, 1275 York Ave, 10065, New York, New York, USA

[6] Radiation Oncology, University of Michigan – Ann Arbor, 1500 E Medical Center Dr., 48109, Ann Arbor, Michigan, USA

3.1 – Abstract

Purpose – RIPF is a chronic, adverse side-effect of lung irradiation exposure characterized by increased collagen deposition and disrupted interstitial structures leading to a thickening of the alveolar walls. The use of stem cells has become a potential treatment modality for RIPF by mitigating local inflammation caused by widespread apoptotic cell death. The purpose of this study is to confirm that MSCs have therapeutic potential in alleviating RIPF and compare the RIPF outcomes of different stem cell administration and recruitment modalities. We will also present an automated quantitative method for histopathological RIPF assessment and compare it to a gold standard certified pathologist scoring.

Methods - Twenty-five rats were separated into five groups: sham-irradiation control (CG), irradiated control (CR), drug treated using granulocyte-macrophage colony stimulating factor or GM-CSF (Drug), intravascularly administered MSC therapy (IV), and intratracheally administered MSC therapy (IT). All rats from all groups, except CG, received 18Gy in one fraction using 6MV photon beam to the right lung. Rat position was verified via cone-beam computed-tomography (CBCT) imaging. Drug, IV and IT groups were given their respective treatments immediately after irradiation. CG and CR groups received no treatment to ameliorate radiation damage. Rats were then sacrificed twenty-four weeks post-irradiation, their lungs fixed, paraffin embedded and stained with Masson's Trichrome. Stained samples were anonymized and scored by a certified pathologist using the modified Ashcroft Scale as a grade from 0 to 8. For the automated analysis, samples were digitized and analyzed using color thresholding to isolate and quantify areas of aniline blue, with large airways and vessels excluded from analysis. Differences between treatment group were tested by variance component analysis and mixed models. Analysis of association between the pathologist scoring and the automated analysis scoring was conducted, and two binary classifiers were trained using the pathologist scoring outcomes,

with 2/3 of the dataset as training and rest as testing set, to assess the ability of automated scores to discriminate between severe and mild grades of RIPF.

Results – DRUG group achieved statistical significantly better outcomes (mean pathologist scoring of 3.96 when compared to other RIPF treatment modalities, performing significantly better than the IV modality (lower by 0.97, p=0.047, 95% confidence interval = [0.013, 1.918]) and resulting in a significant improvement over the CR group (lower by 0.93, p=0.037, 95% confidence interval = [0.062, 1.800]). The IT group also produced significant differences from CR but did not produce significantly better results than the drug group (with a mean pathologist score of 4.25). Algorithm scoring for a pathologist scoring of 4 was 0.225 ± 0.177 (95% prediction interval), with a 0.116 ($p<0.0001$) increase per each 1-unit increase in pathologist scoring, as predicted by the linear regression model. For pathologist scoring of 1 to 3, the predicted algorithm scoring was 0.191 ± 0.167 (95% prediction interval), showing no association between the two scoring methods (p=0.634). Both naïve Bayes and fit discriminator classifiers performed similarly well on the testing set (AUC = 0.923, sensitivity = 0.907, specificity = 0.824).

Conclusion – The use of MSCs can be effective in reducing the severity of RIPF. Among the modalities of administration and recruitment, the use of GM-CSF was the most effective in reducing RIPF. Intravenous administration of MSCs does not appear to be effective at reducing RIPF severity. Automated histological analysis, quantifying amounts of a color of interest, can be used as a surrogate for pathologist scoring and shows potential. In its current form, our automated analysis is only effective for scoring the extent and not denseness of RIPF. In the future, incorporating a level of quantifying structural change due to RIPF can improve this novel method of scoring.

3.2 – Introduction

For patients undergoing thoracic RT, RIPF is an important, permanent, late toxicity of the lung and is one of the most common reasons for reducing treatment intensity which, as a result, jeopardizes the therapeutic effects of RT [1]. It is clinically characterized as a thickening and stiffening of the alveolar walls, much like scarring, resulting from the chronic cellular apoptosis of lung tissues caused by ionizing radiation. The condition is chronic, manifests late, from six to twelve months post-RT, and is permanent after manifestation [2-4]. The development and presentation of RIPF remains poorly understood, varying widely among patients: some individuals exhibit quick progression towards severe outcomes while others present asymptomatically despite similar treatment intensity [1].

Post-irradiation, free radical production and direct deposition of radiation into local DNA, lipids and proteins damages these elements and causes a DNA metabolism disturbance. This triggers transient or permanent cell-cycle arrest or apoptotic cell death [5]. Type-I and type-II pneumocytes sustain the greatest damage [6]. After irradiation, it is thought that type-I cells are denuded, and the proliferation of type-II pneumocytes is stimulated to initiate repair. However, irradiation also induces senescence of the type-II pneumocytes, resulting in a defective repair mechanism, which replaces functional type-I pneumocytes with non-functional fibrotic tissue. Globally, this process of repair is accompanied by chronic local inflammation and secretion of cytokines and growth factors which initiate a restructuring of the extracellular matrix, promoting the production and deposition of collagen. The loss of endothelial cells further increases local inflammation and further promotes the secretion of growth factors and proteases involved in tissue repair, eliciting repair processes and the degradation of extracellular matrix and removal of debris [7]. In general, it is believed that prolonged damage from inflammation and the loss of vital cells contributes to tissue remodeling and tissue replacement by

collagen, leading to the RIPF characteristics of thickening and stiffening of the interstitial structures and loss of pulmonary function [4, 8].

Despite the risks that RIPF poses for patients, there are no FDA approved treatments targeting the underlying molecular processes described [8]. Current therapies attempt to reduce symptoms of RIPF and are generally ineffective. For example, anti-inflammatory therapy has been used extensively to treat radiation injury; corticosteroids and non-steroidal anti-inflammatory drugs are of value in the pre-fibrotic phase and in reducing the acute inflammation potentially associated with fibrosis. But signs and symptoms may recur after the cessation of corticosteroid therapy, and prophylactic administration of corticosteroids does not appear to be beneficial [9]. Other therapies, such as vascular therapy with pentoxifylline or hyperbaric oxygen; treatment with antioxidants like superoxide dismutase, vitamin E (alpha-tocopherol), and a pentoxifylline and vitamin E combination can only act to reduce free radicals, doing little to mitigate RIPF; as a result, therapeutic benefits to patients are few and varied [9].

However, using stem cells to treat RIPF holds promise. MSCs have shown to be of therapeutic value in similar fibrotic diseases [10]. The main proposed mechanisms through which MSCs carry out their reparative effects, following tissue damage, include the capacity of homing to sites of injury due to local release of chemokines [11], the ability to release anti-inflammatory soluble factors, and immunomodulatory properties [10, 12]. These properties appear capable of countering or suppressing many of the defunct and chronic processes which promote the development of RIPF. Furthermore, MSCs, being multipotent cells, have potential to differentiate into a variety of cell types [13] giving them the potential to regenerate, through engraftment, differentiate and replace local cell populations [14]. While engraftment and retention has not been shown to correlate with functional improvement [15], it is possible that temporarily replacing local cell populations may exert a positive effect locally

[14]. The immunomodulation caused by MSCs, through the increased expression of anti-inflammatory cytokines and paracrine effects have been demonstrated in acute kidney [11], liver [16], and lung [17] injury animal models and animals models of sepsis [18], chemical damage [19] and physical damage [20].

In specifically treating RIPF, the literature reports that the main method of action is through replacing lost pneumocytes by differentiation of MSCs [21] and taking advantage of the MSCs' immunomodulatory properties. It has been reported that 15% of MSCs administered, in an *in vivo* mouse model utilizing 2×10^5 MSCs intravenously injected via the tail vein soon after irradiation, will differentiate into type-II pneumocytes and replenish lost pneumocytes [6]. The administration of MSCs and their localization to sites of injury has been shown to be beneficial to injured organs [22-24] including the lungs [25, 26]. MSCs have demonstrable efficacy in reducing bleomycin induced pulmonary fibrosis when administered via the tail vein [14, 27] and intratracheally [28]. Beyond the administration of allogeneic MSCs, there is the interesting alternative of using granulocyte-macrophage colony stimulating factor (GM-CSF) to induce the mobilization of endogenous MSCs to sites of injury. The therapeutic capabilities of GM-CSF have been reported to reduce the severity of lung injury [29] and bacterial lung infection [30].

Despite many studies demonstrating therapeutic effects of administration and the mechanisms of MSC action, there are no studies comparing the different modes of MSC administration and how they impact the therapeutic outcomes with regards to RIPF. In this study, we compared the therapeutic effects on RIPF outcomes of different MSC administration and recruitment methods. We compared intravascular and intratracheal administration, and the recruitment of endogenous stem cells via GM-CSF, in a rat model of RIPF. We also attempted to validate an automated quantitative method of histological RIPF assessment compared to a certified pathologist assessment.

3.3 – Materials and Methods

Animal Preparation

The Animal Care and Use Committee of McGill University approved the animal protocol. Twenty-five pathogen-free female Sprague Dawley rats (Charles River Laboratories, QC, CA), aged 7 to 8 weeks, weighing 200-300 g, were housed in the institution's animal facility. Animals were fed food and water *ad libitum*. After an acclimation period of one week after arrival, animals were randomly assigned into 5 experimental groups with 5 rats per group (n=5): control group given no irradiation (CG); control group given radiation without any treatment intervention (CR); one group treated with granulocyte-macrophage colony stimulating factor or GM-CSF (drug); one group given intravascular administration of 1 x 10^6 MSCs (IV); and one group given intratracheal administration of 2 x 10^5 MSCs (IT).

One week before irradiation, baseline CT scans were taken for radiation treatment planning. For this purpose, all the groups except the CG group were induced to anesthesia with Isoflurane. Once under anesthesia, the animals were imaged on a Philips Brilliance Big Bore CT simulation scanner (Philips Medical Systems, Bothell, Washington, USA) following an optimized small animal protocol (120 kVp X-ray tube voltage, 175 mA tube current, 0.37 mm in-plane resolution, 0.8 mm axial resolution). The animals were placed in a prone position on an in-house built Styrofoam holder with reference markers for positioning reproducibility. The baseline CT scan was used for treatment planning and both lungs were segmented (into lower, middle and upper thirds), and the lungs, heart and spinal cord were contoured on the CT images. An example of a treatment plan is shown in Figure 3.3.1. A single fraction of 18 Gy was prescribed to the right lung using a 6 MV photon beam (Novalis Tx linear accelerator). A hemi-thorax parallel-opposed 3D conformal treatment plan was designed (Eclipse™

V 11.0) for each individual animal based on the CT image. Each plan was adapted to the individual animal's anatomy to spare the spinal cord, heart and left lung. An example of the beam's eye view is shown in Figure 3.3.2. The prescribed dose was delivered using the Novalis Tx linear accelerator (Varian Medical Systems, Palo Alto, California, USA). Anesthetized rats were positioned relative to the markers established at the planning CT. For each rat prior to irradiation, final positioning accuracy was established using cone beam CT. Follow-up pulmonary CT imaging was taken every two weeks for a total of 24 weeks, when the rats were euthanized.

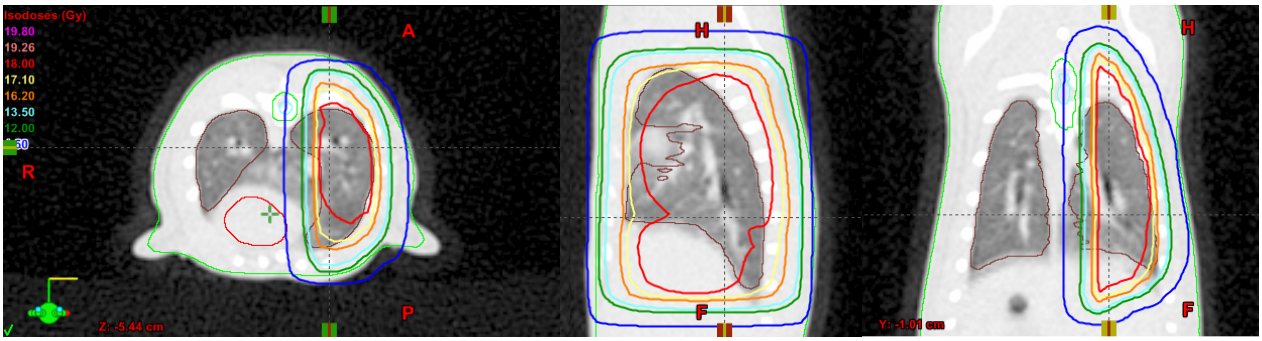

Fig. 3.3.1 – Visualization of an animal treatment plan in the transverse (left), sagittal (middle) and coronal plane (right). Image includes dose distributions, with isodose line values indicated in the image (left), as well as contours for the lungs, spinal cord, spinal cord planning risk volume (PRV) and liver.

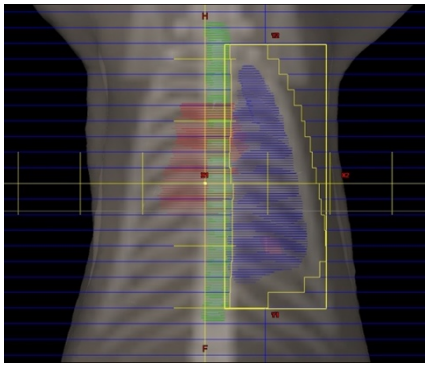

Fig. 3.3.2 – Beams eye view featuring the outline of the treated lung (blue), spinal cord PRV (green) and heart (red) as well as the multi-leaf collimator and leaf positions (identified by the lateral yellow outline and the blue bars, respectively).

Immediately after irradiation the rats received the following treatment intervention: the Drug group received an initial intraperitoneal dose of 10 μg/Kg of GM-CSF followed by a daily administration of the same dose for a total of 7 days [31]. The IT and IV groups received 2 x 10^5 and 1 x 10^6 cells respectively, immediately after irradiation and once every week after irradiation for a total of 6 weeks. The number of cells injected was chosen based on previous studies using IV administration [23, 27] and IT administration [32, 33] and pilot studies which determined the safe amount of cells to be injected.

Histological Preparation

In preparation for sample fixation, the rats were euthanized by CO_2 asphyxiation, after anesthetization with isoflurane, 24 weeks post-irradiation. The chest cavity was opened, and the lungs were removed, washed in PBS and fixed immediately in 10% paraformaldehyde for further processing. Lungs were transversally segmented into upper, middle and lower lobes, paraffin embedded and sectioned. The accessory lobe, when encountered, was not kept for analysis due to its negligible size and inconsistent presence within the population.

For preparation of histological analysis, lung section slides were de-paraffinized, rehydrated through a graded alcohol series, and stained with Masson's Trichrome following the manufacturer's protocol [34]. At the end of the staining, slides were dehydrated through a graded alcohol series, cleared in xylene and mounted. In total, there were 150 slides prepared via this method, with each slide containing 2-3 tissue sections from the same region. Seven additional slides were prepared, following the same methods, in circumstances to supplement slides that had less than 2 intact or well-preserved samples, due to accidental damage, improper storage or improper fixation.

Pathologist Scoring

A certified pathologist scored RIPF in all 157 collected lung sections, stained with Masson's Trichrome, from 25 different animals, using the modified Ashcroft Scale [35]. Samples were anonymized prior to scoring. Given the heterogenous and patchy presence of RIPF, the worst region is given a grade based on the modified Ashcroft Scale, from 0 to 8, following the criteria stipulated under the modified Ashcroft Scale, using a 20-fold objective optimized for histological assessment of pulmonary fibrosis [35]. The modified Ashcroft was used due to its reported precision in the differentiation of RIPF severities and high degree of inter- and intra-observer agreement in comparison to traditional Ashcroft or Wagner scales [35].

Software Analysis

Images of the same 157 prepared samples were acquired at 20x magnification (Figure 3.3.3) using a whole slide scanning technique (Aperio™ Leica Biosystems, USA). The captured images were then imported to and analyzed using ImageScope (Leica Biosystems, USA) with predetermined and preset parameters for specific hue, saturation and brightness (HSB) detection, with a Hue Value (Center) of 0.6, Hue Width of 0.19, and Color Saturation Threshold of 0, and specific output formats. Prior to quantitative analysis, images were contoured to remove all major vessels and airways roughly greater than 250μm in diameter, leaving only the alveolar regions with small vessels and airways for analysis.

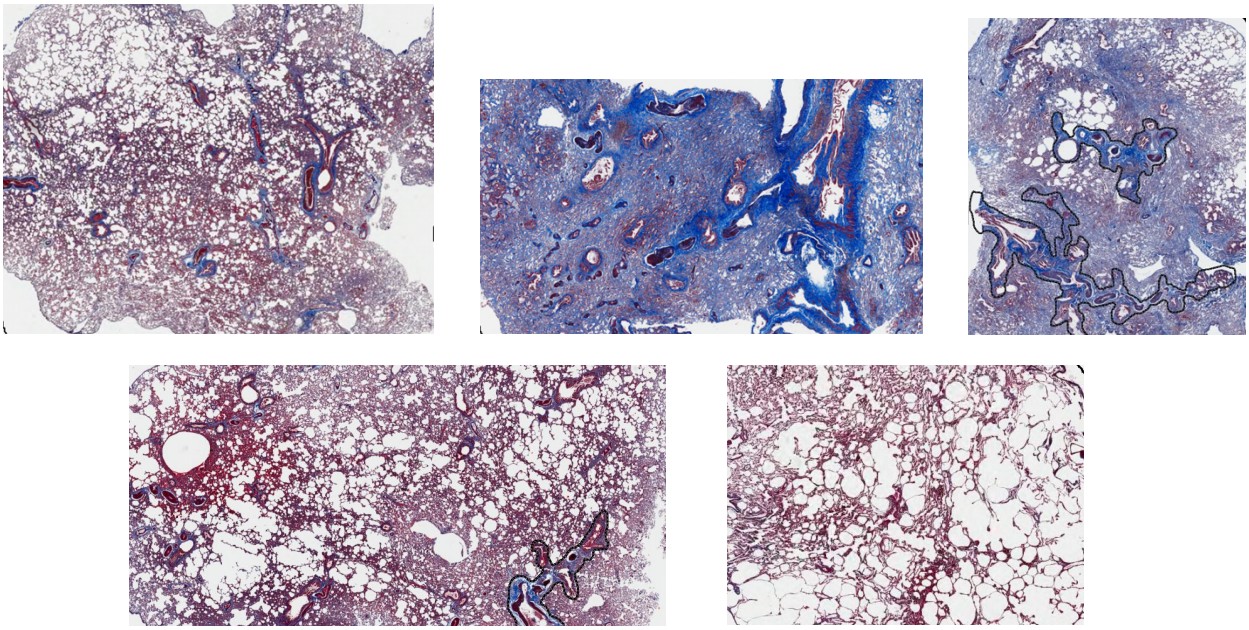

Fig. 3.3.3 – Images of Masson's Trichrome stained lung samples from each group: CG (top left), CR (top middle), DRUG (top right), IV (bottom left) and IT (bottom right).

Each image was analyzed for RIPF by isolating blue-stained regions using color thresholding (Figure 3.3.4), based on a specific HSB value established through a pilot study. N_B represented the number of blue pixels, which was divided by the total area of total tissue N_T, the number of colored pixels, to derive the fraction of blue-stained fibrotic tissue relative to all tissue present (P_R). N_T was obtained through color thresholding of a specific HSB value, determined by a hue value of 0.6 and a hue width of 0.19, which isolates all colored regions, on the image. Within the sample, N_T was indicative of all the tissues included for analysis, and was used to exclude air space from the calculation of P_R.

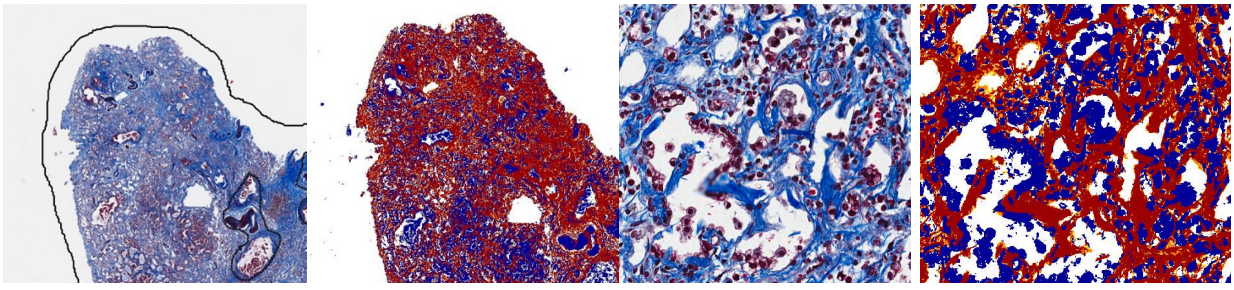

Fig. 3.3.4 – (Above) Images depicting the threshold analysis procedure performed by the software. The first alveolar image (first from the left) is analyzed by the software (visualized in the second image from the left) via a system of color thresholding where strong positives (red), positives (orange) and weak positives (yellow) are detected, according to how closely it resembles the HSB value outlined, and are weighted, according to strength, in the final area calculation. The same technique is shown in a magnified field in the two images on the right.

Data Analysis

The qualitative (pathologist) assessment scores provided by the certified pathologist, and the quantitatively assessed P_R values calculated by the ImageScope software, with predetermined parameters, were assigned to the 5 treatment groups. Data was analyzed using Stata/IC (v15.1, College Station, Texas, USA) statistical software. Mean differences between the treatment groups was assessed using variance components analysis and mixed models (with treatment group as systematic effect and rat as random effect). Group scoring means and 95% confidence interval of the mean were calculated. A p-value$<$0.05 was considered significant. The association between pathologist scoring and algorithm scoring (P_R) is assessed by limits of agreement (95% prediction intervals) using a linear regression model. Naïve Bayes and Fit Discriminator binary classifiers were trained, using an in-house developed MATLAB code (R2018a, MathWorks, Massachusetts, USA) using P_R value to predict pathologist scoring binned into two categories; mild (including grades of 0 to 4 on the modified Ashcroft) and severe (including grades of 5-8). Ratios of mild to severe cases were kept consistent between training and testing sets with two thirds of the data set randomly appointed to be used as the training cohort and the rest as testing.

3.4 – Results

Despite the modified Ashcroft scale offering nine distinct grades, the certified pathologist did not score grades of either 0 or 8 for any of the 157 samples from 25 separate animals. Table 3.4.1 and Figure 3.4.1 provide a summary of the results of the pathologist's scoring.

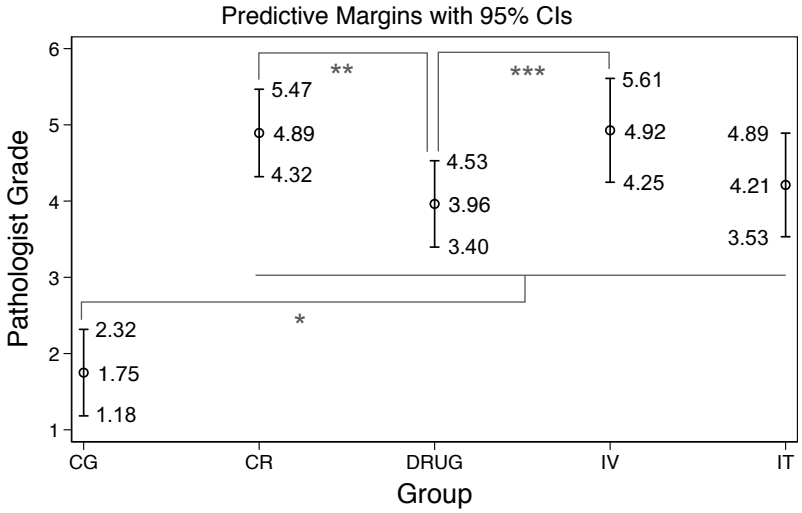

Figure 3.4.1 – Mean of the modified Ashcroft Scale scores for each treatment group, presented with a 95% CI for the mean value, as assessed by a certified pathologist. Significant differences between groups (as indicated in Table 3.4.1) are signified by the asterix.

	Pathologist scoring mean difference	95% CI	p-value
CR vs CG	**3.14**	**[2.274, 4.014]**	**0.000**
DRUG vs CG	**2.21**	**[1.347, 3.079]**	**0.000**
IV vs CG	**3.18**	**[2.225, 4.132]**	**0.000**
IT vs CG	**2.46**	**[1.511, 3.414]**	**0.000**
DRUG vs CR	**-0.93**	**[-1.800, -0.062]**	**0.037**
IV vs CR	0.03	[-0.921, 0.991]	0.940

IT vs CR	-0.68	[-1.636, 0.272]	0.151
IV vs DRUG	**0.97**	**[0.013, 1.918]**	**0.047**
IT vs DRG	0.25	[-0.701, 1.199]	0.589
IT vs IV	-0.72	[-1.747, 0.315]	0.162

Table. 3.4.1 – Pathologist scoring mean differences between treatment groups with 95% CIs and corresponding p-values estimated by the mixed model. Statistically significant differences are indicated in bold.

The quantitative method of assessment produced results that largely differed from the pathologist scoring. The results of the quantitative assessments demonstrated no significant differences between the treatment groups and the irradiated control group (Table 3.4.2 and Figure 3.4.2).

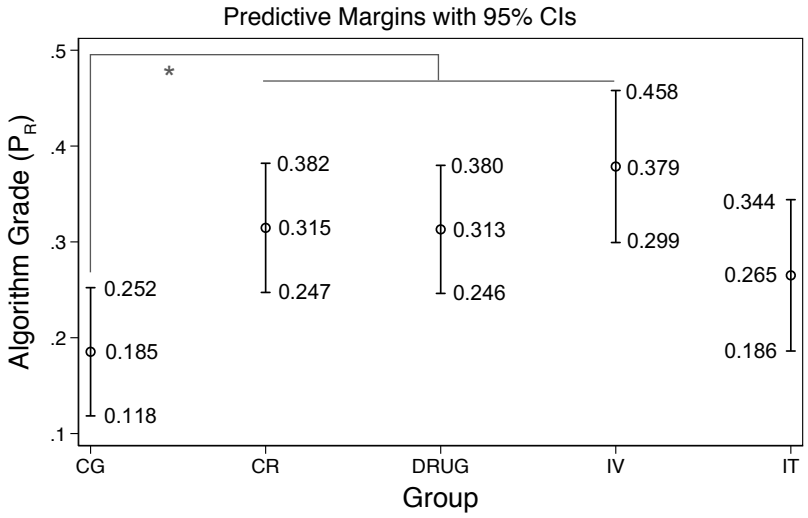

Fig. 3.4.2 – Mean of P_R value for each treatment group, presented with a 95% CI for the mean value, as assessed using predetermined parameters for hue and saturation in ImageScope. Significant differences between groups (as indicated in Table 3.4.2) are signified by the asterix.

	Algorithm scoring mean difference	95% CI	p-value
CR vs CG	**0.129**	**[0.027, 0.232]**	**0.016**
DRUG vs CG	**0.128**	**[0.026, 0.230]**	**0.017**
IV vs CG	**0.193**	**[0.082, 0.305]**	**0.002**
IT vs CG	0.080	[-0.031, 0.191]	0.149
DRUG vs CR	-0.002	[-0.104, -0.101]	0.974
IV vs CR	0.064	[-0.048, 0.176]	0.244
IT vs CR	-0.050	[-0.161, 0.062]	0.362
IV vs DRUG	0.066	[-0.046, 0.177]	0.232

Table. 3.4.2 –Algorithm scoring mean differences between treatment groups with 95% CIs and corresponding p-values estimated by the mixed model. Statistically significant differences are indicated in bold

Pathologist grading, via the modified Ashcroft scale, was associated with that of the P_R value derived from our algorithmic analysis (Figure 3.4.3). Pathologist scoring and P_R value were also plotted with a fitted line and 95% predictive intervals (Figure 3.4.3). There appears to be agreement between pathologist scoring and P_R for pathologist grades from 4 to 7. Lower pathologist graded samples do not have agreement.

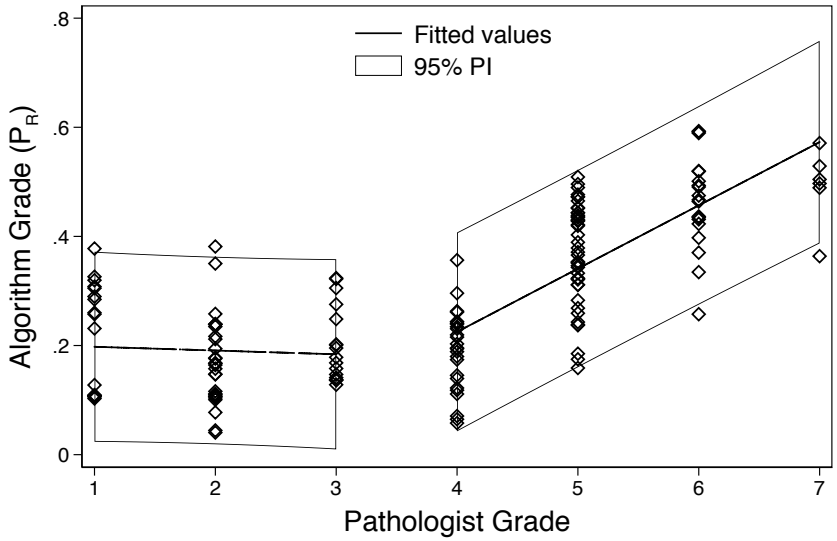

Fig. 3.4.3 – Plot showing the association between pathologist scoring, via the modified Ashcroft Scale, and P_R values for all graded patients. Each point represents an assessed sample with the x-axis value indicating the pathologist score and the y-axis value indicating the P_R value. The best fitting linear regression line and the 95% prediction interval (PI) are displayed.

Analysis of the binary classification ability for P_R scoring indicated that, on the testing set, the naïve Bayes model performed slightly better than the fit discriminator (Figure 3.4.4) in terms of specificity. Overall, both the naïve Bayes and fit discriminator performed similarly in terms of area under the receiver operating characteristic curve (AUC) outcomes and sensitivity.

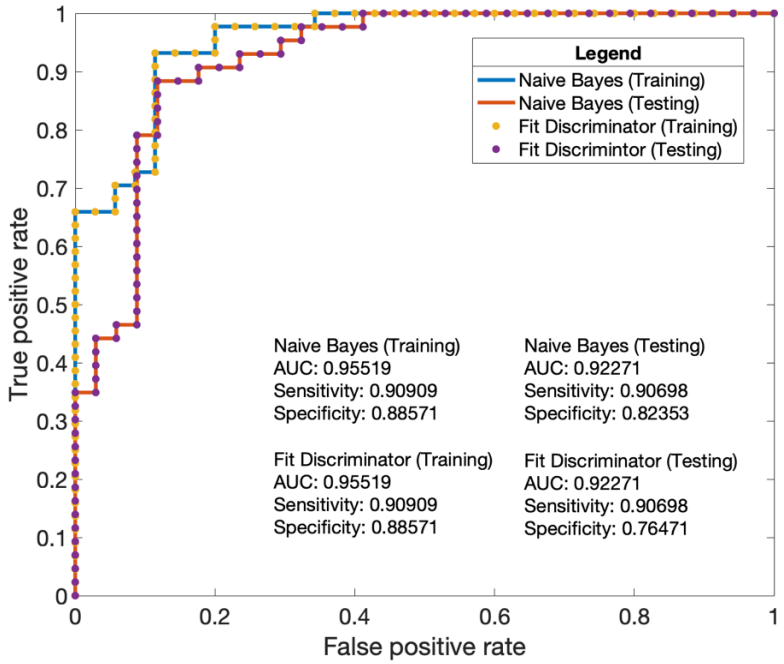

Figure 3.4.4 – Analysis of the binary classification ability for P_R scoring. The two classifiers performed similarly on both the training and testing set, with the naïve Bayes classifier (blue line and red line) performing similarly. With the naïve Bayes (red line) performing slightly better than the fit discriminator (purple dot) on the testing set.

3.5 – Discussions

Overall, stem cell therapy has reduced the severity of RIPF outcomes. The method of MSC administration/recruitment, however, offered different levels of therapeutic benefit. Here we compared different administration/recruitments routes of autologous MSCs and their therapeutic potential in improving RIPF outcomes. We found that the greatest benefit is derived from GM-CSF, with intratracheal administered MSCs being the second most effective in reducing fibrosis.

These findings support the notion that stem cells provide a viable method of reducing RIPF severity and confirm results from previous studies that GM-CSF has therapeutic effects, when applied to a rat model of radiation fibrosis. Further studies comparing GM-CSF's effects with that of other forms of conventional treatments, such as corticosteroids or hyperbaric oxygen should be pursued in animal models to compare and understand the therapeutic potential of GM-CSF and the mechanisms which contribute to its efficacy.

It was notable to find that intravenous injection of MSCs appears to be the *least* effective of the three treatments, causing no discernable improvement in fibrosis outcome, even though this technique is favored in pre-clinical and clinical toxicity mitigation studies [36]. Despite our initial counter-intuitive observation, there may be a theoretical reason for the unexpected outcome. Foremost, there are reports of MSCs causing vascular obstruction [37], with about 80% of MSCs entrapped in the lung's capillary beds [38]. Such a high rate of entrapment has been observed to cause lung embolisms [37] which, in our study, actually resulted in the death of a few animals (data not shown). This prompted adjustments to the protocol by reducing the number of injected MSCs and using MSCs from early passages to counter size increases with increasing passages [39, 40]. This forced a reduction in therapeutic efficacy and brought to light other potential complications that could arise due to

aggregation of MSCs, such as formation of calcium deposits within capillaries [41]. There are also reports of MSCs contributing to chronic inflammation and fibrosis development [6, 42]. More studies should be undertaken to explore how intravenous infusions of MSCs act therapeutically.

Within this study, we also introduced a novel quantitative assessment that uses the area of fibrotic regions, as stained by aniline blue, and compared it with a gold standard assessment done by a certified pathologist. While the method was able to effectively distinguish between cases of extremely severe (modified Ashcroft grade > 4) and non-severe fibrosis (Figure 3.4.4), it was not as capable of discerning between more closely related RIPF severities (Table 3.4.2 and Figure 3.4.2). We hypothesize that this is likely because the color driven quantitative analysis is insensitive to changes of the interstitial structures. For example, the condition of the alveolar septa and of the overall alveoli structures are key indicators for RIPF severity [35]. While the quantitative scoring method we proposed is not sufficiently sensitive enough to match or exceed the pathologist's scoring performance, the scoring method can make for a great supplemental system of quality control or triaging, being that it's automatable, able to assess the condition of entire samples, as opposed to specific areas limited by the viewfinder, and very capable of differentiating between presence and absence of or between very severe and non-severe conditions of RIPF. Such a quantitative technique does have weaknesses, as it is susceptible to confounding factors such as inconsistencies in tissue processing, variations in stain intensities and inconsistent inflation during sample fixation that a subjective observer can accommodate. However, overall, this technique makes a strong case for the utility and capability of quantitative RIPF assessment but also the need for analysis which considers structural changes in addition to pure color measurements.

3.6 – Conclusions

MSC administration and use has demonstrated that it can be effective in reducing the severity of RIPF after ionizing radiation damage to the lung. GM-CSF may be the most effective in reducing RIPF severity followed closely by the intratracheal mode of administration. Intravenous administration of MSCs does not appear to be effective at reducing RIPF severity. Quantitative image analysis may help assessment of therapeutic interventions for RIPF.

3.7 – Acknowledgement

Many thanks to Dr. Jessica Perez for assisting with the animal imaging and irradiation.

3.8 – References

1. Ghafoori, P., et al., *Radiation-induced lung injury. Assessment, management, and prevention.* Oncology (Williston Park), 2008. **22**(1): p. 37-47; discussion 52-3.
2. Bronova, I., et al., *Protection from Radiation-Induced Pulmonary Fibrosis by Peripheral Targeting of Cannabinoid Receptor-1.* Am J Respir Cell Mol Biol, 2015. **53**(4): p. 555-62.
3. Mukherjee, D., et al., *Responses to ionizing radiation mediated by inflammatory mechanisms.* J Pathol, 2014. **232**(3): p. 289-99.
4. Williams, J.P., C.J. Johnston, and J.N. Finkelstein, *Treatment for radiation-induced pulmonary late effects: spoiled for choice or looking in the wrong direction?* Curr Drug Targets, 2010. **11**(11): p. 1386-94.
5. Zhao, W. and M.E. Robbins, *Inflammation and chronic oxidative stress in radiation-induced late normal tissue injury: therapeutic implications.* Curr Med Chem, 2009. **16**(2): p. 130-43.

6. Yan, X., et al., *Injured microenvironment directly guides the differentiation of engrafted Flk-1(+) mesenchymal stem cell in lung.* Exp Hematol, 2007. **35**(9): p. 1466-75.

7. Trott, K.R., T. Herrmann, and M. Kasper, *Target cells in radiation pneumopathy.* Int J Radiat Oncol Biol Phys, 2004. **58**(2): p. 463-9.

8. Beach, T.A., et al., *Radiation induced pulmonary fibrosis as a model of progressive fibrosis: Contributions of DNA damage, inflammatory response and cellular senescence genes.* Exp Lung Res, 2017. **43**(3): p. 134-149.

9. Westbury, C.B. and J.R. Yarnold, *Radiation fibrosis--current clinical and therapeutic perspectives.* Clin Oncol (R Coll Radiol), 2012. **24**(10): p. 657-72.

10. Voswinkel, J., et al., *Use of mesenchymal stem cells (MSC) in chronic inflammatory fistulizing and fibrotic diseases: a comprehensive review.* Clin Rev Allergy Immunol, 2013. **45**(2): p. 180-92.

11. Togel, F., et al., *Administered mesenchymal stem cells protect against ischemic acute renal failure through differentiation-independent mechanisms.* Am J Physiol Renal Physiol, 2005. **289**(1): p. F31-42.

12. Monsel, A., et al., *Cell-based therapy for acute organ injury: preclinical evidence and ongoing clinical trials using mesenchymal stem cells.* Anesthesiology, 2014. **121**(5): p. 1099-121.

13. Cook, D. and P. Genever, *Regulation of mesenchymal stem cell differentiation.* Adv Exp Med Biol, 2013. **786**: p. 213-29.

14. Huang, K., et al., *Conversion of bone marrow mesenchymal stem cells into type II alveolar epithelial cells reduces pulmonary fibrosis by decreasing oxidative stress in rats.* Mol Med Rep, 2015. **11**(3): p. 1685-92.

15. Zheng, G., et al., *Mesenchymal Stromal Cells Affect Disease Outcomes via Macrophage Polarization.* Stem Cells Int, 2015. **2015**: p. 989473.

16. Burra, P., et al., *Systemic administration of a novel human umbilical cord mesenchymal stem cells population accelerates the resolution of acute liver injury.* BMC Gastroenterol, 2012. **12**: p. 88.

17. Xu, J., et al., *Prevention of endotoxin-induced systemic response by bone marrow-derived mesenchymal stem cells in mice.* Am J Physiol Lung Cell Mol Physiol, 2007. **293**(1): p. L131-41.

18. Mei, S.H., et al., *Mesenchymal stem cells reduce inflammation while enhancing bacterial clearance and improving survival in sepsis.* Am J Respir Crit Care Med, 2010. **182**(8): p. 1047-57.

19. Tsai, H.L., et al., *Amelioration of paraquat-induced pulmonary injury by mesenchymal stem cells.* Cell Transplant, 2013. **22**(9): p. 1667-81.

20. Zhao, Y., et al., *Therapeutic effects of bone marrow-derived mesenchymal stem cells on pulmonary impact injury complicated with endotoxemia in rats.* Int Immunopharmacol, 2013. **15**(2): p. 246-53.

21. Theise, N.D., et al., *Radiation pneumonitis in mice: a severe injury model for pneumocyte engraftment from bone marrow.* Exp Hematol, 2002. **30**(11): p. 1333-8.

22. Mastro-Martinez, I., et al., *Effects of local administration of allogenic adipose tissue-derived mesenchymal stem cells on functional recovery in experimental traumatic brain injury.* Brain Inj, 2015. **29**(12): p. 1497-510.

23. Huang, S., et al., *An improved protocol for isolation and culture of mesenchymal stem cells from mouse bone marrow.* J Orthop Translat, 2015. **3**(1): p. 26-33.

24. Moscoso, I., et al., *Analysis of different routes of administration of heterologous 5-azacytidine-treated mesenchymal stem cells in a porcine model of myocardial infarction.* Transplant Proc, 2009. **41**(6): p. 2273-5.

25. Shen, Q., et al., *Paracrine factors from mesenchymal stem cells attenuate epithelial injury and lung fibrosis.* Mol Med Rep, 2015. **11**(4): p. 2831-7.

26. Hayes, M., et al., *Therapeutic efficacy of human mesenchymal stromal cells in the repair of established ventilator-induced lung injury in the rat.* Anesthesiology, 2015. **122**(2): p. 363-73.

27. Sabry, M.M., et al., *Histolgical and immunohistochemical study on the effect of stem cell therapy on bleomycin induced pulmonary fibrosis in albino rat.* Int J Stem Cells, 2014. **7**(1): p. 33-42.

28. Lan, Y.W., et al., *Hypoxia-preconditioned mesenchymal stem cells attenuate bleomycin-induced pulmonary fibrosis.* Stem Cell Res Ther, 2015. **6**: p. 97.

29. Rojas, M., et al., *Bone marrow-derived mesenchymal stem cells in repair of the injured lung.* Am J Respir Cell Mol Biol, 2005. **33**(2): p. 145-52.

30. Lee, J.W., et al., *Therapeutic effects of human mesenchymal stem cells in ex vivo human lungs injured with live bacteria.* Am J Respir Crit Care Med, 2013. **187**(7): p. 751-60.

31. Caraceni, P., et al., *Effects of granulocyte colony stimulating-factor in a rat model of acute liver injury.* Dig Liver Dis, 2007. **39**(10): p. 943-51.

32. Baber, S.R., et al., *Intratracheal mesenchymal stem cell administration attenuates monocrotaline-induced pulmonary hypertension and endothelial dysfunction.* Am J Physiol Heart Circ Physiol, 2007. **292**(2): p. H1120-8.

33. Yu, S.H., et al., *Inhibition of bleomycin-induced pulmonary fibrosis by bone marrow-derived mesenchymal stem cells might be mediated by decreasing MMP9, TIMP-1, INF-gamma and TGF-beta.* Cell Biochem Funct, 2015. **33**(6): p. 356-66.

34. EMS, *Masson's Trichrome for Connective Tissue*, in *Technical Data Sheets*, E.M. Sciences, Editor. 2019, Electron Microscopy Sciences: Electron Microscopy Sciences.

35. Hubner, R.H., et al., *Standardized quantification of pulmonary fibrosis in histological samples.* Biotechniques, 2008. **44**(4): p. 507-11, 514-7.

36. Lalu, M.M., et al., *Safety of cell therapy with mesenchymal stromal cells (SafeCell): a systematic review and meta-analysis of clinical trials.* PLoS One, 2012. **7**(10): p. e47559.

37. Furlani, D., et al., *Is the intravascular administration of mesenchymal stem cells safe? Mesenchymal stem cells and intravital microscopy.* Microvasc Res, 2009. **77**(3): p. 370-6.

38. Lee, R.H., et al., *Intravenous hMSCs improve myocardial infarction in mice because cells embolized in lung are activated to secrete the anti-inflammatory protein TSG-6.* Cell Stem Cell, 2009. **5**(1): p. 54-63.

39. Lo Surdo, J. and S.R. Bauer, *Quantitative approaches to detect donor and passage differences in adipogenic potential and clonogenicity in human bone marrow-derived mesenchymal stem cells.* Tissue Eng Part C Methods, 2012. **18**(11): p. 877-89.

40. Ge, J., et al., *The size of mesenchymal stem cells is a significant cause of vascular obstructions and stroke.* Stem Cell Rev, 2014. **10**(2): p. 295-303.

41. Kurtz, A., *Mesenchymal stem cell delivery routes and fate.* Int J Stem Cells, 2008. **1**(1): p. 1-7.

42. Maria, O.M., et al., *Mesenchymal Stem Cells Adopt Lung Cell Phenotype in Normal and Radiation-induced Lung Injury Conditions.* Applied Immunohistochemistry & Molecular Morphology, 2015. **24**(4): p. 283-295.

§4 Preface for Manuscript #2

In chapter 5, we attempt to validate the efficacy of more conformal external RT techniques in reducing the severity of RIPF and comparing the efficacy of the different modalities of RT. Here, comparisons were made of RIPF scoring by a group of physicians and scoring derived from quantifying fibrosis in patient CT imaging through the use of radiodensities. We were able to verify that more conformal external beam RT techniques do reduce the severity of RIPF. Furthermore, we validated that our model of an automated and quantitative method of scoring RIPF in CT imaging is feasible and shows potential. But currently lacks the important ability to assess structural changes due to RIPF.

§5 Comparing the radiation induced pulmonary fibrosis outcomes between SBRT, IMRT and 3D-CRT

Li Ming Wang[1,2,*], Alexandre Semionov[3], Avishek Chatterjee[4], James Man Git Tsui[5], Sangkyu Lee[6], Issac Yang[5], Yarab Al Bulushi[5], Jan Seuntjens[4], Norma Ybarra[1,2,4]

* To whom correspondence should be addressed: li.m.wang@mail.mcgill.ca
Phone: 1 (647) 867-4811

Keywords: Radiation induced pulmonary fibrosis (RIPF), External Beam Radiotherapy, 3D Conventional Radiotherapy (3D-CRT), Intensity Modulated Radiotherapy (IMRT), Stereotactic Body Radiotherapy (SBRT)

Running title: Comparing the radiation induced pulmonary fibrosis outcomes between SBRT, IMRT and 3D-CRT

[1] Cancer Research Program, Research Institute of the McGill University Health Centre, 1001 Décarie Blvd, H4A 3J1, Montréal, Canada

[2] McGill University, 845 Sherbrooke St W, H3A 0G4, Montréal, Canada

[3] Department of Radiology, Royal Victoria Hospital, McGill University Healthcare Centre, 1001 Décarie Blvd, H4A 3J1, Montréal, Canada

[4] Medical Physics Unit, Cedars Cancer Centre, McGill University Healthcare Centre, 1001 Décarie Blvd, H4A 3J1, Montréal, Canada

[5] Department of Radiation Oncology, Cedars Cancer Centre, McGill University Healthcare Centre, 1001 Décarie Blvd, H4A 3J1, Montréal, Canada

[6] Memorial Sloan Kettering Cancer Centre, 1275 York Ave, 10065, New York, New York, USA

5.1 – Abstract

Purpose - Sparing healthy lung tissue during RT has been shown to reduce the severity of RIPF. SBRT and IMRT offer the possibility of reducing dose to healthy tissue through better dose distribution and more conformal fields. In this study, we attempted to validate the benefit of conformal techniques in reducing RIPF severity through comparing outcomes assessed via a traditional physician scoring and a novel automated analysis based on changes in radiodensity.

Methods - RT patients with non-small cell lung cancer (86 total) received conventional RT (n=43), IMRT (n=13) or SBRT (n=30) treatment. Patients were scored for RIPF, defined by changes between CT imaging acquired six-months post-treatment and pre-treatment; changes were measured by a group of physicians via a five-grade criterion and an automated algorithm detecting radiodensity changes. A two-sample T-test was then performed to verify significant differences between grade distributions.

Results - Results of the physician scoring indicated that the RIPF resulting from patients being treated with SBRT (mean grade of 1.4000 with a 95% confidence interval between 1.0005 and 1.7995) was significantly lower ($p<0.05$) than both Conventional RT and IMRT (mean grade of 2.0233 with a 95% confidence interval between 1.6176 and 2.4289 and 2.0000 with a 95% confidence interval between 1.4484 and 2.5516 respectively). The automated analysis indicated that the conformal techniques, a combined group featuring SBRT and IMRT, were associated with significantly better RIPF outcomes (mean score of -0.0162 with a 95% confidence interval between -0.0533 and 0.0209) compared with 3D-CRT (mean score of 0.0595 with a 95% confidence interval between -0.0077 and 0.1267). The correlation between the two scoring methods was significant and the values were 0.71, 0.59, 0.68 and 0.64, for the Conventional, IMRT, SBRT group and all groups combined, respectively.

Conclusions - SBRT is a superior modality of treatment when compared to 3D-CRT and IMRT with respect to RIPF outcome. While the results derived from the automated analysis are promising, they do contradict physician appraisals and highlight the need to improve our automated approach for assessing RIPF, as the feature of radiodensity changes alone is not sufficient.

5.2 – Introduction

RIPF is a late and permanent complication of thoracic RT characterized by the progressive and permanent formation of scar tissue in the lungs, often leading to reduced lung function [1]. The appearance of RIPF will permanently deplete the already limited pulmonary reserves of NSCLC patients who have undergone treatment. While the use of large doses of ionizing radiation to target NSCLC lesions improves tumor and disease control and reduces the likelihood of recurrence, the increased doses also introduce larger amounts of radiation into surrounding healthy tissues. Over the years, many studies have demonstrated the efficacy of decreasing dose to healthy tissues as a way of reducing the severity of RIPF and other RT treatment toxicities [2-5]. Hence, modern RT techniques, such as SBRT and IMRT, offer an opportunity to minimize doses to healthy tissues while maximizing doses to target volumes [6].

SBRT, which has also been referred to as stereotactic ablative radiotherapy (SABR), is a method of delivering therapeutic and ablative doses of radiation to target volumes with highly conformal, sub-millimeter, precision [7]. This precision not only allows larger doses of radiation to be given per fraction, but also allows the entire dose to be delivered in a shorter period of time, enabling greater tumor control while sparing greater amount of the surrounding healthy tissues [7, 8]. SBRT has been reported to decrease certain lung toxicities, such as pneumonitis [9-11], and there is reason to believe that SBRT can reduce RIPF as well.

Alternatively, IMRT, which uses fluctuating beam intensities during the course of treatment, is able to apply reduced beam intensities where beam tracks cross specific OAR. This reduces dose deposition into healthy tissues, OARs and allows for more conformal delivery of radiation, specifically on structures with concave curvature [12] in addition to also delivering reduced doses to structures

outside of target volumes. However, unlike SBRT, IMRT does not offer the large doses per fraction or accelerated treatment schedules and cannot offer similar sub-millimeter precision. However, it is the more forgiving modality due to the large number of fractions and is more capable at delivering therapeutic doses to targets with large degrees of movement. There are studies indicating that IMRT outperforms SBRT in genitourinary toxicity outcomes for RT used to treat prostate cancers [8] giving credence to its potential as a possible modality which can improve pulmonary toxicities as well.

In the past decade, we see more utilization of automated conformal techniques, such as SBRT and IMRT in efforts to reduce toxicity to OARs. However, literature has not shown that these conformal techniques improves RIPF outcomes. Many of the studies attempting to capture, score and use pulmonary adverse events as a study outcome, such as RIPF, encounter great difficulty due to lack of accuracy, replicability and objectivity in scoring methods [13-15] or are retrospective in nature. Conventional scoring of RIPF, and other acute or chronic pulmonary side effects, have been repeatedly verified in the literature as being highly variable and difficult to score with a diverse range of different clinical definitions for severities [16-18] that can vary between physicians and institutions. Hence, the purpose of this prospective study is to investigate, through manual scoring of RIPF, whether conformal techniques, such as SBRT and IMRT, improve RIPF outcomes. We also attempt to validate a novel technique for an automated and quantitative RIPF scoring, through the use of an engineered imaging biomarker, to assess if a quantitative approach is comparable to a physician in its ability to identify RIPF outcomes.

5.3 – Materials and Methods

Patient Cohort

The study was approved by the Ethics Committee of the McGill University Healthcare Center. Patients were treated at the Montreal General Hospital and Cedars Cancer Centre were included in the study based one of the three following criteria for RT: 1) Conventional RT treated with a combination chemotherapy using carboplatin, gemcitabine, taxol, vinorelbine, docetaxel, trastuzumab, etoposide, pemetrexed or a combination of these chemotherapeutic agents, 2) treated on an static field SBRT protocol, 3) or treated with an IMRT protocol which utilizes volumetric modulated arc therapy (VMAT). Neither IMRT nor SBRT patients received concomitant chemotherapy.

Patients were enrolled into this prospective study if they were: 1) Diagnosed with primary non-small cell lung cancer, regardless of previous malignancy history, 2) scheduled to receive radical radiotherapy to the thorax as a part of their treatment with or without chemo or targeted therapy, 3) not candidates for resection, 3) scored >60 on the Karnofsky Performance status, 4) 18 years old or older and 5) are willing and able to provide informed consent. Patients' oncological data and treatment data were collected. Patients were excluded if they: 1) Have a history of prior lung irradiation, 2) are pregnant or nursing and 3) have a survival estimation of under 6 months.

All pre-treatment CT images were taken on a CT Big Bore (Phillips, USA) and were used for the CT simulation and treatment planning. All follow-up diagnostic CT imaging were conducted at institutions of the patients choosing, with imaging taken using a variety of machines, ranging from the Aquilion ONE (Canon Medical Systems, USA), Discovery ST (GE Healthcare), Discovery PET/CT710 (GE Healthcare), Discovery CT750 HD (GE Healthcare), Ingenuity CT (Phillips, USA), Lightspeed VCT (GE Healthcare), Revolution EVO (GE Healthcare) and SOMATOM Definition Flash + (Siemens Healthcare, USA).

Physician Scoring

Four physicians (a staff radiologist with cardiothoracic fellowship training, a radiation oncology resident and two radiology residents) scored the severity of RIPF after six-month post-treatment using a set of anonymized images which involved the planning CT images before treatment and diagnostic CT images at six months post-treatment. RIPF is based on a five-grade scale: with grade 0 being no fibrosis, grade 1 being less than or equal to one pulmonary segment equivalent of fibrosis (PSEF), grade 2 being greater than one but less than or equal to 2 PSEF, grade 3 being more than 2 PSEF and grade 4 being the involvement of more than one pulmonary lobe (Table 5.3.1). One PSEF is defined as roughly the volume of half the right middle lung lobe. The mode score of the four physicians (S_P) was used as the scoring for any given patient.

Grade 0	Grade 1	Grade 2	Grade 3	Grade 4
0 PSEF	≦1 PSEF	≧1 PSEF, ≦2 PSEF	≧2 PSEF	≧1 pulmonary lobe affected

Table 5.3.1 – A summary of the grading scale used by the physician in scoring the severity of RIPF. It is based on a measure of a pulmonary segment equivalent of fibrosis (PSEF) and the volume of a PSEF is relative to the volume of the patients right middle lobe.

Image Analysis

For the automated analysis, post-treatment images, at six months, were deformably registered to pre-treatment CTs using an in-house algorithm developed in MevisLab™. This initial step allowed us to overcome some potential scanner differences between planning and follow-up diagnostic images [19]. For either the treated lung, defined as the ipsilateral lung, and the non-treated lung, defined as the contralateral lung, the voxel HU counts were binned as histograms for the irradiated lung parenchyma (total treated lung volume minus the PTV). The distributions of the post-treatment contralateral

density distribution were corrected with the pre-treatment contralateral density distribution. The correction value was defined as the translation applied to the post-treatment contralateral distribution which, when computed in a cross-correlation with the pre-treatment contralateral distribution, yielded the lowest sum. This correction value was then applied to the post-treatment ipsilateral lung distribution (Figure 5.3.1). This allows us to correct for global and bilateral opacities and density increase that are not characteristic of RIPF, such as chemo induced pneumonitis as well as scanner differences. The difference between follow-up and baseline histograms were computed and used as the quantitative measure of RIPF (S_D) and its area normalized to unity. The difference was calculated at empirically determined density range of RIPF, defined as the fibrotic window. The density range was determined through a physician aided measurements of HU densities for RIPF in 10 test images. This window was established so as to exclude diffuse opacities which could be due to atelectasis or temporary inflammations.

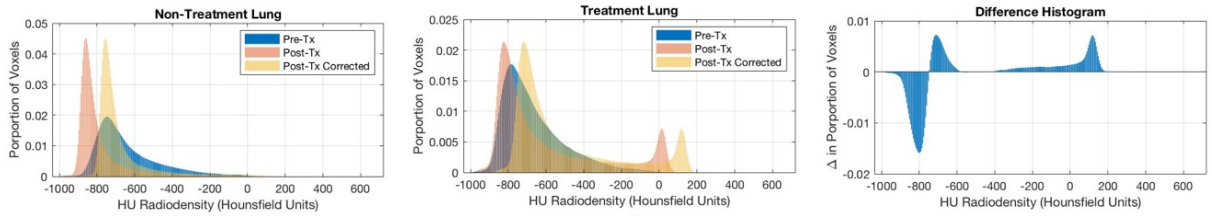

Figure 5.3.1 – The correction, after initial registration is outlined in the above figure. First, in the non-treatment lung, the post-treatment (Post-Tx, colored orange) is translated (Post-Tx Corrected, colored yellow) to match the pre-treatment distribution (Pre-Tx, colored blue). The appropriate translation is calculated as the translation of Post-Tx which produces the lowest sum in a sliding dot product of Post-Tx and Pre-Tx. This correction value generated for the non-treatment lung is then applied to the Post-Tx of the treatment lung to create the Post-Tx Corrected distribution. The difference is then generated between Post-Tx Corrected and Pre-Tx for the treatment lung. S_D is the area between the fibrotic window normalized to unity.

Data Analysis

For the analysis, two-sample t-tests were performed to verify significance between scoring distributions for treatment groups for both S_P and S_D. Analysis was conducted using MATLAB™.

5.4 – Results

A total of eighty-six patients were enrolled into the study between 2008 and 2016. Characteristics of the patient cohort as well as disease specifics are summarized in Table 5.4.1.

	Conventional RT (n=43, 50.6%)	IMRT (n=13, 14.9%)	SBRT (n=30, 34.5%)
Age Mean	64.1	67.5	73.7
Range	39 - 83	57 - 92	59 - 88
Sex			
Male	21 (48.8%)	6 (46.2%)	21 (70.0%)
Female	22 (51.2%)	7 (53.8%)	9 (30.0%)
Dose			
Total Dose	58.7 (±3.5)Gy	58.3 (±9.6)Gy	45.4 (±7.4)Gy
Number of Fractions	27.9 (±5.2)	25.1 (±7.0)	5.5 (±5.2)
Gy/Fraction	2.2 (±0.52)	2.5 (±0.72)	13.7 (±8.35)
Histology			
Adenocarcinoma	22 (51.2%)	6 (46.2%)	12 (40.0%)
Squamous cell	11 (25.6%)	4 (30.7%)	6 (20.0%)
Unknown	9 (20.9%)	2 (15.4%)	10 (33.3%)
Other	1 (2.3%)	1 (7.7%)	2 (6.7%)
Tumor Staging			
Ia	0	1 (7.7%)	12 (40.0%)
Ib	2 (4.7%)	0	7 (23.3%)
IIa	1 (2.3%)	0	1 (3.3%)
IIb	3 (7.0%)	2 (15.3%)	1 (3.3%)
IIIa	21 (48.8%)	5 (38.5%)	2 (6.7%)
IIIb	16 (37.2%)	5 (38.5%)	2 (6.7%)
IIIc	0	0	0
IVa	0	0	0
IVb	0	0	0
N/A	0	0	5 (16.7%)
Disease Metastasis	19 (44.2%)	5 (38.5%)	6 (20%)
Tumor Location			
Left Lung			
Upper Lobe	12 (27.8%)	4 (30.7%)	10 (33.3%)
Lower Lobe	4 (9.3%)	2 (15.4%)	2 (6.7%)
Hilar	2 (4.7%)	0 (0.0%)	0 (0.0%)
Right Lung			
Upper Lobe	13 (30.2%)	2 (15.4%)	9 (30.0%)
Middle Lobe	2 (4.7%)	0 (0.0%)	2 (6.7%)
Lower Lobe	8 (18.6%)	3 (23.1%)	6 (20.0%)
Hilar	0 (0.0%)	2 (15.4%)	0 (0.0%)
Mediastinal	2 (4.7%)	0 (0.0%)	1 (3.3%)
COPD	9 (20.9%)	3 (23.1%)	14 (46.7%)
Unsure	2 (4.7%)	2 (15.4%)	0 (0.0%)
Smoking			
Currently	9 (20.9%)	3 (23.1%)	2 (6.7%)

Quit	31 (72.1%)	7 (53.8%)	23 (76.7%)
Never	3 (7.0%)	1 (7.7%)	4 (13.3%)
Unknown	0 (0.0%)	2 (15.4%)	1 (3.3%)
Use of Steroidal Anti-inflammatory			
Yes	18 (41.9%)	4 (30.8%)	8 (26.7%)
Unknown	2 (4.7%)	1 (7.7%)	6 (20.0%)

Table 5.4.1 – Summary of patient demographic and characteristics. Under Histology, 'Other' is indicative of primary or secondary disease that has been confirmed to be something other than adenocarcinoma or squamous cell carcinoma. 'Unknown' is indicative of unspecified pathology due to early stage disease or undifferentiating biopsies despite continuation with treatment. Disease Metastasis indicates eventual metastatic disease detected at a later period, during a follow-up, post-treatment. This is differentiated from stage IV cases that identify metastatic disease prior to first treatment consultation or during treatment.

From our empirical analysis, the fibrotic window was determined to be between -271.5 and 188.5 HU.

Results of the physician scoring are outlined in Table 5.4.2 and Figure 5.4.1. The S_P distributions of each group were compared using a two-sample t-test, the p-values of which are presented in Figure 2.

SBRT produced significantly better outcomes than both Conventional RT and IMRT.

	Mean (Physician)	CI (95%)
Conventional RT	2.0233	(1.6176, 2.4289)
IMRT	2.0000	(1.4484, 2.5516)
SBRT	1.4000	(1.0005, 1.7995)

Table 5.4.2 – Results of the physician scoring. The 95% CI of the mean is presented under the CI (95%) column.

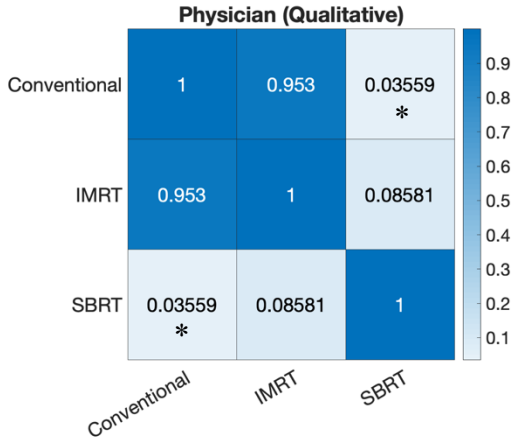

Figure 5.4.1- Results of the two-sample t-test with p-values presented between different treatment groups for S_P grading distributions. Significant values, defined as <0.05, are marked by an Asterix. The gradient bar on the right are p-values corresponding to color.

The Spearman's correlation coefficient, between the S_P and S_D, for the same treatment group, were 0.71, 0.59, 0.68 and 0.64, for the Conventional, IMRT, SBRT and all groups combined, respectively (with p-values all below 0.05).

For the algorithm analysis, in order to improve statistical power due to small sample size, SBRT and IMRT groups were collectively combined for the data analysis due to the lack of significance between S_P RIPF outcomes for IMRT and SBRT, both groups being tissue sparing modalities and both groups, when combined, having equal population numbers as compared to Conventional RT. The results of the analysis for the algorithmic, comparing the two treatment modality groups in S_D, is presenting in Table 5.4.3 and Figure 5.4.2. Conformal techniques, comprising of SBRT and IMRT produced significantly better outcomes than 3D-CRT.

	Mean (Algorithm)	CI (95%)
Conventional RT	0.0595	(0.0077, 0.1267)
SBRT & IMRT	-0.0162	(-0.0533, -0.0209)

Table 5.4.3 - Results of the quantitative algorithm scoring. The 95% CI of the mean is presented under the CI (95%) column.

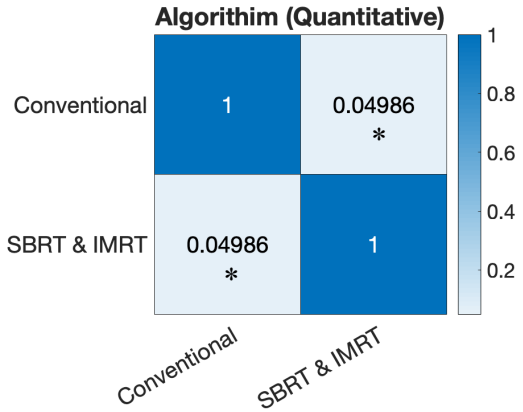

Figure 5.4.2 - Results of the two-sample T-test with p-values presented between different treatment groups for S_D scoring distributions. Significant values, defined as <0.05, are marked by an asterix. The gradient bar on the right are p-values corresponding to color.

5.5 – Discussions

We were able to establish a relationship between tissue sparing RT treatment modalities and improved RIPF outcomes while having proposed and tested a quantitative method of RIPF scoring. To our knowledge, this is the first time this has been done specifically with RIPF and with a relatively heterogenous cohort as most studies have only been able to demonstrate correlation in small homogenous populations [18, 20]. It is also, to our knowledge, the first time that tissue sparing RT modalities are shown, both quantitatively and qualitatively to result in better RIPF outcome in a comparative and prospective study. An important result of our study was that we were able to confirm that tissue sparing modalities are effective in reducing RIPF while also showing that a simple imaging biomarker, in this case radiodensities, is capable of being a surrogate for RIPF if implemented carefully.

We were able to create a methodology and establish, practically, some of the theoretical groundwork by which RIPF can be scored precisely, thoroughly and reproducibly. Recent clinical studies focusing on collecting and utilizing RIPF outcomes have demonstrated that it is not a simple task [13] and that current clinical definition of RIPF [21-23] are not adequate to help accurately, consistently or objectively capture RIPF outcomes for research or to allow for clear comparisons [16]. Even the introduction of patient reported outcomes or symptomologies are not adequate and are subjective [16, 17, 24]. This is largely due to the overlap between (i) symptoms experienced as a result of NSCLC, (ii) symptoms of the other pulmonary side effects associated with RT for NSCLC, (iii) the often asymptomatic presentation of RIPF in NSCLC patients post-RT [6, 25] or (iv) the general improvement in physical condition after recession of primary disease which offsets the appearance of toxicity symptoms [26]. Hence, in order to ultimately study RIPF outcomes given a specific RT

modality, much of the techniques in this study were motivated to overcome this difficulty through the design of engineered qualitative and quantitative scoring method based on objective evidence to reduce subjectivity and variability.

Given the heterogeneity with treatment and primary disease severity within the cohort, there was the need to specifically design both our qualitative and quantitative scoring methodology to overcome many of the scoring issues that have been brought up in literature and in the clinic [16, 18, 27]. While other groups chose to address these problems through the use of more abstract or generally a greater number of biomarkers [17], our method was to pay close attention to the clinical manifestation of possible confounds and address them through the design of our scoring method. This, to our knowledge, is a novel approach.

One of the primary elements that we addressed, which we identified as being capable of disrupting consistent scoring of RIPF is the use of concomitant chemotherapy in the conventional treatment arm. In the literature, chemotherapy has been shown to cause symptoms of pulmonary fibrosis which generally mirrors that of RIPF, producing opacities in CT imaging. However, given that administration of chemotherapy is global, the development of fibrosis, and the development of other forms of increased pulmonary opacity, due to any form of temporary type-II collagen deposition as a result of pneumonitis, or permanently stable collagen type-I deposition due to chemotherapy induced fibrosis would be much more global, diffuse and bilateral [28, 29]. Whereas RIPF only appears within regions specifically touched by ionizing radiation or crossed by treatment beam tracks [6, 7, 30] and appear in delineated, discrete and patchy volumes. These assumptions were considered when we built our qualitative and quantitative scoring protocols.

For the qualitative physician scoring criteria, we utilized a discrete volumetric component, the PSEF unit, requiring assessors to base severity on volume affected. This is in contrast to traditional methods of assessment which evaluates severity based on fibrotic extent proportional to total lung volume [21-23]. The concept of the PSEF unit reinforced the goal of grading RIPF, as opposed to generalized fibrosis, inflammation due to chemotherapy or any other opacity causing interstitial diseases by forcing assessors to grade based on discrete regions of concentrated fibrosis. This meant that graders were specifically identifying patchy regions with typical RIPF characteristics. To reinforce this, physicians were also given pre-treatment planning images for reference, and thus were able to exclude already present diffuse, global and bilateral opacities due to pre-existing conditions or neoadjuvant chemotherapy.

For the quantitative analysis, we first utilized an empirically derived and specific HU range in order to eliminate regions that we believe to have diffuse fibrosis. The empirical range was established through corroborating results of physician appraisal, where a certified radiologist identified the HU density values of select regions that they deemed to be clear instances of RIPF, and a data driven analysis where the results of the physician's mode score were correlated with the quantitative score produced by an in-house algorithm for a variety of different HU ranges in order to ascertain the lower and upper bound of the fibrotic window which yielded the best correlation. These two empirical methods of determining a functional range yielded our fibrotic window standard of -271.5 and 188.5 HU, between which we calculated radiodensity differences. This is the first instance of an empirically established density range for RIPF. Furthermore, in addition to utilizing this predetermined density range to exclude diffuse instances of fibrosis, density correction was also applied to the treatment lung images using the non-treatment lung. This corrected for globalized, diffuse and bilateral density increases

which occur in both lungs, such as that brought about by chemotherapy induced pneumonitis or fibrosis.

Outside of the challenges posed by chemotherapy, the severity and presence of a primary disease can be confounding. Indeed, patients in the 3D-CRT cohort of this study suffer from more severe NSCLC than do the other two groups. Through the design of our scoring method, there were a few ways that we overcame factors posed by the primary disease.

The first of these applicable factors is the effect that physical tumor sizes will have on the quantitative RIPF assessment. In terms of potential for uncharacteristic fibrosis development, larger tumors which undergo successful reduction through treatment will leave larger absences of space for residual tissue healing. However, the subsequent healing and tissue replacement or redistribution in the vacancy left by the shrinking tumor leads to variable radiodensity. There is evidence to suggest that there is a decreased radiodensity in and around the area of the PTV due to expansion of tissue into the vacant volumes left by the tumor [31]. Alternatively, there is also evidence to suggest that there will be increased radiodensities in areas of higher dose with larger PTVs [32]. Theoretically, the biomolecular processes occurring in these fringe areas could result in either a decrease or increase in radiodensity. However, at the moment, there is no consensus or explanation as to if decrease or increase is expected and what mechanisms or conditions could lead to one or the other. While the radiodensity changes in areas of tumor vacancy is important to develop in further research, for the purposes of our study, in trying to avoid the variability this issue poses, our scoring methods specifically excludes the contents of the PTV from analysis. While the purpose of the exclusion is to focus on RIPF which occurs due to tissue sparing around the PTV, it has the complementary benefit of also excluding potential variability due to healing in regions which were occupied by the primary disease.

This exclusion of the PTV is also important if we accept that inflammation in the tumor environment plays a role in contributing to the inflammatory state which can lead to and exacerbate RIPF. It is well known, that the tumor microenvironment is bathed in a complex and unique chronic inflammatory condition which helps feed the growth of the tumor [33]. The aggregation of macrophages, excretion of tumor necrosis factor alpha (TNFα), and many immune modulatory growth factors, such as those in the interleukin family, and transforming growth factor beta (TGF-ß) upregulation in the tumor microenvironment shares similarities to that of the inflammatory and acute stage pneumonitis that is strongly believed to predate RIPF events [6, 30]. Hence, it is a strong assumption to suggest that there is likely a relation between the severity of inflammation in the tumor microenvironment and the severity of RIPF. But, foremost, there is evidence in the literature suggesting that RIPF events may not require previous acute inflammation [25]. And even if we are to assume that inflammation in the tumor microenvironment can predicate RIPF events, the inflammatory reaction which occurs in the tumor environment is only localized to the tumor itself. While this may theoretically lead to increased likelihood and severity of RIPF occurring in and around the tumor or in regions where the tumor has regressed due to treatment [5], it is difficult to assume that inflammation in the tumor microenvironment plays a role in more distal fibrotic events. Currently, there are, to our knowledge, no literature which demonstrates a relation of distal RIPF severity in connection to tumor sizes or NSCLC staging. In fact, a calculation of correlation between cancer staging and RIPF severity in our study cohort did not show any correlation between the two variables. Hence, excluding the PTV from the analysis is, again, an optimal way to remove the potential of variability brought about by the inflammatory tumor microenvironment and the primary disease.

Alternatively, there is the notion that the more intensive treatment is given for the more intensive disease and ought to bring about more intensive side effects. In our study, patients with small

resectable primary tumors of less than 2cm with no nodal involvement were typically SBRT candidates. Advanced cancer stages and infiltrated disease typically received IMRT or 3D-CRT. This could potentially produce increased densities proportional to treatment severity. This is a valid concern. However, after having controlled for the presence of chemotherapeutically induced radiodensity changes and radiodensity changes, which can result from the primary disease's severity, all that remains in affecting treatment intensity is total dose, fractionation and the tissue sparing capabilities of a given treatment modality. With the lung being a late responding tissue, reduction of tissue damage is typically achieved through more numerous fractionations. However, our findings, that SBRT results in reduced RIPF damage, appears to demonstrate that this may not be the case or that RIPF severity is not proportional to cell killing. Regions of the lung that cross SBRT beam tracks should be receiving higher doses which cause greater damage. But this does not appear to translate into increased RIPF severity. In fact, our results seem to indicate that greater fractionation, less dose per fraction over a larger lung volume result in more severe RIPF outcomes. This may support the notion that the repair mechanisms, which lead to RIPF, are actually experiencing some level of defect, wherein moderate tissue damage and cell death is being over-repaired. Within our data, when calculating correlation between both S_P or S_D with either total dose, fractionation number and dose per fraction, there appears to not be any correlation when calculated for each modality separately and when calculated for all eighty-six patients combined. Hence, our result does not support the idea that the more intensive primary disease or the more intensive treatment lead to a worse RIPF outcome. The exclusion of the PTV has also allowed us to ignore the regions which receive the most intense doses, as the regions in the PTV are receiving close to 100% of the necessary tumor control dose, will likely develop RIPF with severity proportional to that of dose.

Another factor which affects our study is the unequal use of steroidal anti-inflammatories among the cohorts, with a larger proportion of Conventionally treated patients taking anti-inflammatories in comparison to the SBRT and IMRT patients. This is largely due to steroidal anti-inflammatories being used to treat the non-tolerable acute side effects of RT [6, 30]. However, there is no indication that the use of steroidal anti-inflammatories has any effect on the development of RIPF [34, 35]. While anti-inflammatories modulate acute phase pneumonitis, it is uncertain that the temporary use of anti-inflammatories for the alleviation of acute pneumonitis truly alleviates states of chronic inflammation which can bring about RIPF [25]. Within our own cohort, there was no relationship between use of steroidal anti-inflammatories and the S_P or S_D when calculated for each modality separately and when calculated for all eighty-six patients combined.

In regard to the automated quantitative scoring, the correlation between S_P and S_D, which had a value of 0.64, is not indisputable but it does show promise for the approach that we used to resolve this long-standing problem of RIPF identification. Practically, 0.64 indicates that our automated quantitative scoring method lacks sensitivity and does have trouble discerning smaller differences between grades, such as that between what a physician would determine to be a grade 1 or 2 but is much more capable at discerning differences between a grade 1 and a grade 4. This level of correlation is in line with other studies that have done similar kinds of correlation between a quantitative method of RIPF scoring and physician scoring [17, 19, 20].

This is a reasonable limitation given that RIPF is characterized by extracellular matrix remodelling and collagen deposition. As such, mere radiodensity increases, reflective of collagen deposition only, are unable to fully differentiate similar severities of RIPF. The radical change in and obliteration of regular interstitial structure often defines the more severe forms of RIPF and can often be the differentiator in scoring. For example, there is another study in the literature, that uses a large quantity of imaging

biomarkers to approximate a type of structural analysis [17]. Our method of deliberately engineering one biomarker lacks this capability, both in design and in quantity of biomarkers used. But engineered biomarker that performs structural analysis with built-in confound exclusions can be built and applied with minimal modification to the methodology we presented.

Given our method of scoring, we are also necessarily limited to identifying RIPF, as opposed to more generalized radiation induced lung damage, as a result of tumorous NSCLC treated through RT. This method of customizing and being deliberate about the use of a small selection of criteria has allowed us to take on greater heterogeneity in terms of comorbidities, disease severities and treatment modalities. But this comes at the cost of limiting our ability to identify only the outcomes of RIPF as opposed to the more common outcome of generalized radiation induced lung injury that is of interest in the literature. This specific focus is a limitation to the method of engineered imaging biomarkers and deliberately designed qualitative scoring criteria. It exposes a very interesting question of whether biomarkers can be overdesigned and so focused that they become a reflection of the intentions of the designer and, in turn, lack the ability to be practically useful. This is an interesting dilemma and more research regarding this matter should be explored with different degrees of biomarker design being compared in terms of their performance and ability to mask objective outcomes.

Ultimately, it is important to participate in a more quantitative and objective tracking of an outcome such as RIPF. The lack of dependable information, from clinical trials, and the difficulty of ensuring objective replicability, due to shortcomings such as the subjective nature of appraisals, should give reasons for tracking. Even though this may contribute to the creation of a wide variety of noncompatible ontologies on the matter, it can lead to fruitful trial-and-error results. It also gives researchers the capability to begin building a basis of knowledge about how to appraise a disease that is permanent, progressive and debilitating in its more severe forms.

The use of biomarkers should also, to an extent, be tailored for the purpose of use. It could be said that using several poorly designed and implemented biomarkers will be just as ineffective as using one or two poorly designed and implemented biomarkers. Quantity does not overcome inappropriate biomarker application. Hence, future studies identifying biomarkers should be attentive to the design of biomarkers and incorporate some level of innate exclusion abilities rather than rely on larger amounts of different biomarkers to overcome confounds. This has the potential of not only resulting in quality biomarkers but also reduced number of total biomarkers, reducing computational needs, input data needs and making implementation and widespread adoption more feasible.

5.6 – Conclusions

Based on the physician scoring, SBRT was able to produce a significant improvement in RIPF outcomes compared to IMRT and 3D-CRT techniques. Based on the quantitative scoring, we were able to demonstrate that tissue sparing treatment modalities also demonstrate a significant improvement in RIPF outcomes. It seems that overall, healthy tissue sparing supports improved RIPF outcomes, in that greater tissue sparing results in reduced RIPF severity in the long term. It is also likely that the accelerated schedule and greater dose per fraction of the SBRT protocol further improves this healthy tissue sparing benefit. Both the quantitative and qualitative technique that we designed appear to help address the ambiguity of current methods in assessing RIPF. With the quantitative method specifically, we were able to build in toxicity exclusions that start to mimic a lot of the physicians' appraisal ability due to experience.

5.7 – References

1. Straub, J.M., et al., *Radiation-induced fibrosis: mechanisms and implications for therapy.* J Cancer Res Clin Oncol, 2015. **141**(11): p. 1985-94.

2. Zhou, C., et al., *Quantitative assessment of radiation dose and fractionation effects on normal tissue by utilizing a novel lung fibrosis index model.* Radiat Oncol, 2017. **12**(1): p. 172.

3. Prasanna, P.G., et al., *Normal tissue protection for improving radiotherapy: Where are the Gaps?* Transl Cancer Res, 2012. **1**(1): p. 35-48.

4. Marks, L.B., et al., *Radiation dose-volume effects in the lung.* Int J Radiat Oncol Biol Phys, 2010. **76**(3 Suppl): p. S70-6.

5. Larici, A.R., et al., *Lung Abnormalities at Multimodality Imaging after Radiation Therapy for Non–Small Cell Lung Cancer.* RadioGraphics, 2011. **31**(3).

6. Simone, C.B., 2nd, *Thoracic Radiation Normal Tissue Injury.* Semin Radiat Oncol, 2017. **27**(4): p. 370-377.

7. Linda, A., M. Trovo, and J.D. Bradley, *Radiation injury of the lung after stereotactic body radiation therapy (SBRT) for lung cancer: a timeline and pattern of CT changes.* Eur J Radiol, 2011. **79**(1): p. 147-54.

8. Yu, J.B., et al., *Stereotactic body radiation therapy versus intensity-modulated radiation therapy for prostate cancer: comparison of toxicity.* J Clin Oncol, 2014. **32**(12): p. 1195-201.

9. Lucas, J.T., Jr., et al., *Comparison of accelerated hypofractionation and stereotactic body radiotherapy for Stage 1 and node negative Stage 2 non-small cell lung cancer (NSCLC).* Lung Cancer, 2014. **85**(1): p. 59-65.

10. Tong, A.N., et al., *Advantages of CyberKnife for inoperable stage I peripheral non-small-cell lung cancer compared to three-dimensional conformal radiotherapy.* Mol Clin Oncol, 2015. **3**(2): p. 442-448.

11. Nyman, J., et al., *SPACE - A randomized study of SBRT vs conventional fractionated radiotherapy in medically inoperable stage I NSCLC.* Radiother Oncol, 2016. **121**(1): p. 1-8.

12. Cho, B., *Intensity-modulated radiation therapy: a review with a physics perspective.* Radiat Oncol J, 2018. **36**(1): p. 1-10.

13. Chiang, A., et al., *A comparison between accelerated hypofractionation and stereotactic ablative radiotherapy (SABR) for early-stage non-small cell lung cancer (NSCLC): Results of a propensity score-matched analysis.* Radiother Oncol, 2016. **118**(3): p. 478-84.

14. Koshy, M., et al., *Stereotactic body radiotherapy and treatment at a high volume facility is associated with improved survival in patients with inoperable stage I non-small cell lung cancer.* Radiother Oncol, 2015. **114**(2): p. 148-54.

15. Yirmibesoglu, E., et al., *Challenges scoring radiation pneumonitis in patients irradiated for lung cancer.* Lung Cancer, 2012. **76**(3): p. 350-3.

16. Faria, S.L., et al., *The challenge of scoring radiation-induced lung toxicity.* Clin Oncol (R Coll Radiol), 2009. **21**(5): p. 371-5.

17. Veiga, C., et al., *Novel CT-Based Objective Imaging Biomarkers of Long-Term Radiation-Induced Lung Damage.* Int J Radiat Oncol Biol Phys, 2018. **102**(4): p. 1287-1298.

18. De Ruysscher, D., et al., *Quantification of radiation-induced lung damage with CT scans: the possible benefit for radiogenomics.* Acta Oncol, 2013. **52**(7): p. 1405-10.

19. Palma, D.A., et al., *A new approach to quantifying lung damage after stereotactic body radiation therapy.* Acta Oncol, 2011. **50**(4): p. 509-17.

20. Ghobadi, G., et al., *A new CT-based method to quantify radiation-induced lung damage in patients.* Radiother Oncol, 2015. **117**(1): p. 4-8.

21. *Common Terminology Criteria for Adverse Events (CTCAE) Version 5.0*, U.S.D.o.H.a.H. Services, Editor. 2017.

22. Cox, J.D., J. Stetz, and T.F. Pajak, *Toxicity criteria of the Radiation Therapy Oncology Group (RTOG) and the European Organization for Research and Treatment of Cancer (EORTC).* Int J Radiat Oncol Biol Phys, 1995. **31**(5): p. 1341-6.

23. Pavy, J.J., et al., *EORTC Late Effects Working Group. Late Effects toxicity scoring: the SOMA scale.* Int J Radiat Oncol Biol Phys, 1995. **31**(5): p. 1043-7.

24. Heo, J., et al., *CT-based quantitative evaluation of radiation-induced lung fibrosis: a study of interobserver and intraobserver variations.* Radiat Oncol J, 2014. **32**(1): p. 43-7.

25. McDonald, S., et al., *Injury to the lung from cancer therapy: Clinical syndromes, measurable endpoints, and potential scoring systems.* International Journal of Radiation Oncology Biology and Physics, 1995. **31**(5): p. 1187-1203.

26. Jaen, J., et al., *Long-term changes in pulmonary function after incidental lung irradiation for breast cancer: a prospective study with 7-year follow-up.* Int J Radiat Oncol Biol Phys, 2012. **84**(5): p. e565-70.

27. Ghafoori, P., et al., *Radiation-induced lung injury. Assessment, management, and prevention.* Oncology (Williston Park), 2008. **22**(1): p. 37-47; discussion 52-3.

28. Boiselle, P.M., M.M. Morrin, and M.S. Huberman, *Gemcitabine pulmonary toxicity: CT features.* J Comput Assist Tomogr, 2000. **24**(6): p. 977-80.

29. Tamura, M., et al., *High-resolution computed tomography findings for patients with drug-induced pulmonary toxicity, with special reference to hypersensitivity pneumonitis-like patterns in gemcitabine-induced cases.* Oncologist, 2013. **18**(4): p. 454-9.

30. Williams, J.P., C.J. Johnston, and J.N. Finkelstein, *Treatment for radiation-induced pulmonary late effects: spoiled for choice or looking in the wrong direction?* Curr Drug Targets, 2010. **11**(11): p. 1386-94.

31. Diot, Q., et al., *Regional normal lung tissue density changes in patients treated with stereotactic body radiation therapy for lung tumors.* Int J Radiat Oncol Biol Phys, 2012. **84**(4): p. 1024-30.

32. Phernambucq, E.C., et al., *Time and dose-related changes in radiological lung density after concurrent chemoradiotherapy for lung cancer.* Lung Cancer, 2011. **74**(3): p. 451-6.

33. Gomes, M., et al., *The role of inflammation in lung cancer.* Adv Exp Med Biol, 2014. **816**: p. 1-23.

34. Molls, M., et al., *Radiopathology of the lung: experimental and clinical observations.* Recent Results Cancer Res, 1993. **130**: p. 109-21.

35. Kwok, E. and C.K. Chan, *Corticosteroids and azathioprine do not prevent radiation-induced lung injury.* Can Respir J, 1998. **5**(3): p. 211-4.

§6 General Discussion

In this work we sought to quantify RIPF in two different studies, one being the histopathological identification of RIPF in a rat model and the other being a CT identification of RIPF in NSCLC patients who received RT. The two studies were able to demonstrate that quantitative measures, when applied in a specific and deliberate way, show promise in being able to adequately score RIPF severity. Our quantitative approach was able to achieve similar levels of performance to the physicians for RIPF appraisal and scoring tasks although there is much room for improvement.

The application of specifically designing quantitative biomarkers, to more closely resemble the features that a physician observer would look for, remains an interesting method of approach. This type of technique relies on translating qualitative features into quantifiable variables. Within the scope of our projects, this meant translating the qualitative features associated with the presence, extent and severity of RIPF into a quantification of area that exhibit a specific HSB value of blue, in histopathology, and a quantification of the volume within a CT image which falls between a range of radio-densities associated with RIPF. This translation from qualitative appraisal to quantitative appraisal opens up the possibility to streamline the RIPF scoring process, reducing the need for specialists and instead utilizing automated techniques to perform the work. The use of quantifiable variables also allows for the implementation of built-in exclusions. In our case, it allowed for the exclusion of non-fibrotic regions, such as related opacity caused by toxicities that visually look similarly to RIPF but are indicative of disease or comorbidities other than RIPF. For example, within the histopathological sample, the exclusion of other colours that were close to blue, such as purple, allowed for the precise exclusion of regions occupied by inflammatory cells ensuring that we are only quantifying regions of clearly identifiable fibrosis. In the prospective patient study, the exclusion of the PTV and instances of generalized, bilateral and global fibrosis like densities, through the correction of the follow-up

imaging with the pre-treatment imaging, allowed for the exclusion of potential confounding opacities associated with the primary disease and chemo related pneumonitis. This level of customization offers the ability to be more precise in identifying and quantifying features of interest. And allows for highly reproducible and consistent appraisals after the establishment of a set of analysis criteria at the beginning of the study.

6.1 - Limitations

The act of customizing biomarkers does fall risk to the potential of being overdesigned. While the ultimate goal of this project was to develop a more objective method of RIPF scoring, we were still unsuccessful in removing subjectivity from the process. While we were able to ensure that subjectivity no longer affects the reproducibility of scoring, by removing the need for a unique subjective interpretation for every new image or sample set, we have reallocated the use of subjectivity to a more global role. Wherein subjectivity is now used to specify and design the biomarker of interest that will be automatically quantified. While removing subjectivity from each individual instance of appraisal ensures that the scoring can be reproducible, moving subjectivity into a design role also means that it now has a potentially greater role in establishing how features are assessed. That is to say a bias at the stage of biomarker design would become a global bias that carries itself through every iteration of scoring. This could hamper the validity of entire studies based around this methodology if the design is questionable.

In addition, in the current state, the use of a single customized biomarker with exclusions, such as that of area of blue in the histopathological study and the volume of a certain HU radio-density, is not practical. The single biomarker, regardless of precision in its design, is unable to be a surrogate for physician appraisals. With the use of one specifically designed biomarker, quantitative methods are

not effective in being adequate RIPF quantifying systems. They cannot capture enough detail or information to allow for the differentiation between more minute differences that are obvious to a physician observer. Throughout the two studies, it is abundantly clear that RIPF is multifaceted in its presentation and appears with, often, many other visually confounding opacities. The use of a single modality, no matter how well designed, is just not assessing enough information that are vital to RIPF identification. Thus, in both studies, we mentioned the necessity for a quantitative measure of structural distortion that RIPF causes. A plausible method to achieve this would be to utilize a form of image registration which can capture the movement of specific anatomical landmarks between baseline and follow-up imaging

Finally, while the samples sizes offered in each of the two manuscripts, 5 rats and 86 patients, are modest in size, they are nevertheless not large enough to achieve significant statistical conclusions or have general clinical significance. However, the methods presented in this thesis can be applied to a larger quantity of animals or patients in order to validate designed biomarkers or the value of a colorimetric or radiodensity driven model of RIPF assessment. The addition and incorporation of other designed biomarkers, such as those that are sensitive to structural changes, can help extend the current assessment capabilities of the protocols set forth in this thesis without the need for excessive alterations. Overall, the methodologies developed in this thesis, while being used in the manuscript in a limited capacity and limited efficacy, can be adapted and improved upon to produce more significant, realistic and objective assessments of RIPF.

§7 Conclusion

Being able to identify instances of RIPF in a replicable and objective manner is of great importance to the reduction of side effects resulting from radiation treatment for lung cancers. Traditional methods of assessment lack the objectivity and reproducibility of quantitative methods which can utilize consistent diagnostic elements in order to derive a score for RIPF severity. Quantitative methods also have the added ability of being very adaptable, being easily configured to observe for specific characteristics and be easily automatable. Being able to better consistently and accurately identify RIPF can allow more precise outcome analysis in research regarding late effects of radiation and can be used in the clinic to help clinicians better identify and track a patient's risk for complication as well as the development of complication.

This thesis presented two circumstances in which an objective and automated method of scoring RIPF was applied. The first of the two manuscripts attempted to validate a colorimetric driven quantification of stained collagen in a RIPF induced rat model. The second of the two manuscripts attempted to validate a radiodensity driven quantification of RIPF events retrospectively on a group of NSCLC patients. Both of these studies revealed that the method of deliberately designing a biomarker with specific exclusion shows promise in being able to score specific sequalae like RIPF. However, in its current stages, these techniques lack the necessary sensitivity to be usable in a clinical setting. In both of the quantitative scoring techniques, there lacked an element of structural assessment leading to the conclusion that there must be some level of sensitivity for structural changes in order for quantitative assessments of RIPF to be effective. In addition, the reliance on a singular property, whether that would be color or radio-density, no matter how well designed it is to exclude potential confounds, will still be inadequate and overreliance can lead to biased assessments, deviating away from the goal of objectivity.

7.1 - Outlook

By these efforts, future studies can explore designed biomarkers as a possible means of developing reliable outcomes. Designing biomarkers offers a potential means of improving the quality of outcomes data that studies utilize, ensuring that outcomes are collected and segregated in a consistent and reproducible manner. Alternatively, the automation of the RIPF scoring process can be applied in clinic with minimal alterations to the role of current clinical staff. Once a criterion for RIPF scoring is established, a clinic can implement algorithms which automatically generate plausible scoring for patients who have follow-up imaging. The algorithm in question would not operate much more differently than what was highlighted within our study. This could potentially improve detection of RIPF for future NSCLC patients who undergo radiotherapeutic treatment.

§8 General References

1. Jaffray, D.A. and M.K. Gospodarowicz, *Radiation Therapy for Cancer*, in *Cancer: Disease Control Priorities, Third Edition (Volume 3)*, H. Gelband, et al., Editors. 2015, The International Bank for Reconstruction and Development / The World Bank: Washington (DC).
2. Straub, J.M., et al., *Radiation-induced fibrosis: mechanisms and implications for therapy.* J Cancer Res Clin Oncol, 2015. **141**(11): p. 1985-94.
3. Baskar, R., et al., *Cancer and radiation therapy: current advances and future directions.* Int J Med Sci, 2012. **9**(3): p. 193-9.
4. Phernambucq, E.C., et al., *Time and dose-related changes in radiological lung density after concurrent chemoradiotherapy for lung cancer.* Lung Cancer, 2011. **74**(3): p. 451-6.
5. Jassem, J., *Combined chemotherapy and radiation in locally advanced non-small-cell lung cancer.* Lancet Oncol, 2001. **2**(6): p. 335-42.
6. Cho, B., *Intensity-modulated radiation therapy: a review with a physics perspective.* Radiat Oncol J, 2018. **36**(1): p. 1-10.
7. Yu, J.B., et al., *Stereotactic body radiation therapy versus intensity-modulated radiation therapy for prostate cancer: comparison of toxicity.* J Clin Oncol, 2014. **32**(12): p. 1195-201.
8. Guckenberger, M., et al., *Pulmonary injury and tumor response after stereotactic body radiotherapy (SBRT): results of a serial follow-up CT study.* Radiother Oncol, 2007. **85**(3): p. 435-42.
9. Linda, A., M. Trovo, and J.D. Bradley, *Radiation injury of the lung after stereotactic body radiation therapy (SBRT) for lung cancer: a timeline and pattern of CT changes.* Eur J Radiol, 2011. **79**(1): p. 147-54.

10. Jeppesen, S.S., et al., *Stereotactic body radiation therapy versus conventional radiation therapy in patients with early stage non-small cell lung cancer: an updated retrospective study on local failure and survival rates.* Acta Oncol, 2013. **52**(7): p. 1552-8.

11. Gutiontov, S.I., et al., *Intensity-Modulated Radiation Therapy (IMRT) for Head and Neck Surgeons.* Head Neck., 2016. **38**: p. E2368-E2373.

12. Aridgides, P., et al., *Clinical outcomes following advanced respiratory motion management (respiratory gating or dynamic tumor tracking) with stereotactic body radiation therapy for stage I non-small-cell lung cancer.* Lung Cancer (Auckl), 2018. **9**: p. 103-110.

13. Wu, Q.J., et al., *The impact of respiratory motion and treatment technique on stereotactic body radiation therapy for liver cancer.* Med Phys, 2008. **35**(4): p. 1440-51.

14. Razzaque, M.S. and T. Taguchi, *Pulmonary fibrosis: cellular and molecular events.* Pathol Int, 2003. **53**(3): p. 133-45.

15. Wynn, T.A., *Cellular and molecular mechanisms of fibrosis.* J Pathol, 2008. **214**(2): p. 199-210.

16. Simone, C.B., 2nd, *Thoracic Radiation Normal Tissue Injury.* Semin Radiat Oncol, 2017. **27**(4): p. 370-377.

17. Beach, T.A., et al., *Radiation induced pulmonary fibrosis as a model of progressive fibrosis: Contributions of DNA damage, inflammatory response and cellular senescence genes.* Exp Lung Res, 2017. **43**(3): p. 134-149.

18. Marks, L.B., et al., *Radiation dose-volume effects in the lung.* Int J Radiat Oncol Biol Phys, 2010. **76**(3 Suppl): p. S70-6.

19. Ghafoori, P., et al., *Radiation-induced lung injury. Assessment, management, and prevention.* Oncology (Williston Park), 2008. **22**(1): p. 37-47; discussion 52-3.

20. Hotchkin, D. *Radiation-Induced Lung Injury*. Radiation-Induced Lung Injury, 2017.

21. Morry, J., W. Ngamcherdtrakul, and W. Yantasee, *Oxidative stress in cancer and fibrosis: Opportunity for therapeutic intervention with antioxidant compounds, enzymes, and nanoparticles.* Redox Biol, 2017. **11**: p. 240-253.

22. Fleckenstein, K., et al., *Temporal onset of hypoxia and oxidative stress after pulmonary irradiation.* Int J Radiat Oncol Biol Phys, 2007. **68**(1): p. 196-204.

23. Zhao, W. and M.E. Robbins, *Inflammation and chronic oxidative stress in radiation-induced late normal tissue injury: therapeutic implications.* Curr Med Chem, 2009. **16**(2): p. 130-43.

24. Yan, X., et al., *Injured microenvironment directly guides the differentiation of engrafted Flk-1(+) mesenchymal stem cell in lung.* Exp Hematol, 2007. **35**(9): p. 1466-75.

25. Deng, G., et al., *Pulmonary toxicity generated from radiotherapeutic treatment of thoracic malignancies.* Oncol Lett, 2017. **14**(1): p. 501-511.

26. Ward, H.E. and T.E. Nicholas, *Alveolar type I and type II cells.* Aust N Z J Med, 1984. **14**(5 Suppl 3): p. 731-4.

27. Williams, J.P., C.J. Johnston, and J.N. Finkelstein, *Treatment for radiation-induced pulmonary late effects: spoiled for choice or looking in the wrong direction?* Curr Drug Targets, 2010. **11**(11): p. 1386-94.

28. Trott, K.R., T. Herrmann, and M. Kasper, *Target cells in radiation pneumopathy.* Int J Radiat Oncol Biol Phys, 2004. **58**(2): p. 463-9.

29. Martini, F.H. and J.L. Nath, *The Respiratory System*, in *Fundamentals of Anatomy & Physiology 8th Edition*. 2008, Benjamin Cummings.

30. Hubner, R.H., et al., *Standardized quantification of pulmonary fibrosis in histological samples.* Biotechniques, 2008. **44**(4): p. 507-11, 514-7.

31. Ashcroft, T., J.M. Simpson, and V. Timbrell, *Simple method of estimating severity of pulmonary fibrosis on a numerical scale.* J Clin Pathol, 1988. **41**(4): p. 467-70.

32. Wang, J., et al., *Pharmacological targeting of BET proteins attenuates radiation-induced lung fibrosis.* Sci Rep, 2018. **8**(1): p. 998.

33. Bronova, I., et al., *Protection from Radiation-Induced Pulmonary Fibrosis by Peripheral Targeting of Cannabinoid Receptor-1.* Am J Respir Cell Mol Biol, 2015. **53**(4): p. 555-62.

34. Mukherjee, D., et al., *Responses to ionizing radiation mediated by inflammatory mechanisms.* J Pathol, 2014. **232**(3): p. 289-99.

35. Faria, S.L., et al., *The challenge of scoring radiation-induced lung toxicity.* Clin Oncol (R Coll Radiol), 2009. **21**(5): p. 371-5.

36. Yirmibesoglu, E., et al., *Challenges scoring radiation pneumonitis in patients irradiated for lung cancer.* Lung Cancer, 2012. **76**(3): p. 350-3.

37. Westbury, C.B. and J.R. Yarnold, *Radiation fibrosis--current clinical and therapeutic perspectives.* Clin Oncol (R Coll Radiol), 2012. **24**(10): p. 657-72.

38. Delanian, S. and J.L. Lefaix, *Current management for late normal tissue injury: radiation-induced fibrosis and necrosis.* Semin Radiat Oncol, 2007. **17**(2): p. 99-107.

39. Afzal, M.R., et al., *Adult Bone Marrow Cell Therapy for Ischemic Heart Disease: Evidence and Insights From Randomized Controlled Trials.* Circ Res, 2015. **117**(6): p. 558-75.

40. Sumita, Y., et al., *Bone marrow-derived cells rescue salivary gland function in mice with head and neck irradiation.* Int J Biochem Cell Biol, 2011. **43**(1): p. 80-7.

41. Voswinkel, J., et al., *Use of mesenchymal stem cells (MSC) in chronic inflammatory fistulizing and fibrotic diseases: a comprehensive review.* Clin Rev Allergy Immunol, 2013. **45**(2): p. 180-92.

42. Herrera, M.B., et al., *Exogenous mesenchymal stem cells localize to the kidney by means of CD44 following acute tubular injury.* Kidney Int, 2007. **72**(4): p. 430-41.

43. Togel, F., et al., *Administered mesenchymal stem cells protect against ischemic acute renal failure through differentiation-independent mechanisms.* Am J Physiol Renal Physiol, 2005. **289**(1): p. F31-42.

44. Monsel, A., et al., *Cell-based therapy for acute organ injury: preclinical evidence and ongoing clinical trials using mesenchymal stem cells.* Anesthesiology, 2014. **121**(5): p. 1099-121.

45. Cook, D. and P. Genever, *Regulation of mesenchymal stem cell differentiation.* Adv Exp Med Biol, 2013. **786**: p. 213-29.

46. Aicher, A., et al., *Assessment of the tissue distribution of transplanted human endothelial progenitor cells by radioactive labeling.* Circulation, 2003. **107**(16): p. 2134-9.

47. Hou, D., et al., *Radiolabeled cell distribution after intramyocardial, intracoronary, and interstitial retrograde coronary venous delivery: implications for current clinical trials.* Circulation, 2005. **112**(9 Suppl): p. I150-6.

48. Zheng, G., et al., *Mesenchymal Stromal Cells Affect Disease Outcomes via Macrophage Polarization.* Stem Cells Int, 2015. **2015**: p. 989473.

49. Burra, P., et al., *Systemic administration of a novel human umbilical cord mesenchymal stem cells population accelerates the resolution of acute liver injury.* BMC Gastroenterol, 2012. **12**: p. 88.

50. Xu, J., et al., *Prevention of endotoxin-induced systemic response by bone marrow-derived mesenchymal stem cells in mice.* Am J Physiol Lung Cell Mol Physiol, 2007. **293**(1): p. L131-41.

51. Yao, Y., et al., *Paracrine action of mesenchymal stem cells revealed by single cell gene profiling in infarcted murine hearts.* PLoS One, 2015. **10**(6): p. e0129164.

52. Huang, W., et al., *Paracrine Factors Secreted by MSCs Promote Astrocyte Survival Associated With GFAP Downregulation After Ischemic Stroke via p38 MAPK and JNK.* J Cell Physiol, 2015. **230**(10): p. 2461-75.

53. Mei, S.H., et al., *Mesenchymal stem cells reduce inflammation while enhancing bacterial clearance and improving survival in sepsis.* Am J Respir Crit Care Med, 2010. **182**(8): p. 1047-57.

54. Tsai, H.L., et al., *Amelioration of paraquat-induced pulmonary injury by mesenchymal stem cells.* Cell Transplant, 2013. **22**(9): p. 1667-81.

55. Zhao, Y., et al., *Therapeutic effects of bone marrow-derived mesenchymal stem cells on pulmonary impact injury complicated with endotoxemia in rats.* Int Immunopharmacol, 2013. **15**(2): p. 246-53.

56. Theise, N.D., et al., *Radiation pneumonitis in mice: a severe injury model for pneumocyte engraftment from bone marrow.* Exp Hematol, 2002. **30**(11): p. 1333-8.

57. Gao, F., et al., *Mesenchymal stem cells and immunomodulation: current status and future prospects.* Cell Death Dis, 2016. **7**: p. e2062.

58. Huang, K., et al., *Conversion of bone marrow mesenchymal stem cells into type II alveolar epithelial cells reduces pulmonary fibrosis by decreasing oxidative stress in rats.* Mol Med Rep, 2015. **11**(3): p. 1685-92.

59. Mastro-Martinez, I., et al., *Effects of local administration of allogenic adipose tissue-derived mesenchymal stem cells on functional recovery in experimental traumatic brain injury.* Brain Inj, 2015. **29**(12): p. 1497-510.

60. Huang, S., et al., *An improved protocol for isolation and culture of mesenchymal stem cells from mouse bone marrow.* J Orthop Translat, 2015. **3**(1): p. 26-33.

61. Moscoso, I., et al., *Analysis of different routes of administration of heterologous 5-azacytidine-treated mesenchymal stem cells in a porcine model of myocardial infarction.* Transplant Proc, 2009. **41**(6): p. 2273-5.

62. Shen, Q., et al., *Paracrine factors from mesenchymal stem cells attenuate epithelial injury and lung fibrosis.* Mol Med Rep, 2015. **11**(4): p. 2831-7.

63. Hayes, M., et al., *Therapeutic efficacy of human mesenchymal stromal cells in the repair of established ventilator-induced lung injury in the rat.* Anesthesiology, 2015. **122**(2): p. 363-73.

64. Sabry, M.M., et al., *Histolgical and immunohistochemical study on the effect of stem cell therapy on bleomycin induced pulmonary fibrosis in albino rat.* Int J Stem Cells, 2014. **7**(1): p. 33-42.

65. Lan, Y.W., et al., *Hypoxia-preconditioned mesenchymal stem cells attenuate bleomycin-induced pulmonary fibrosis.* Stem Cell Res Ther, 2015. **6**: p. 97.

66. Sanganalmath, S.K., et al., *Hematopoietic cytokines for cardiac repair: mobilization of bone marrow cells and beyond.* Basic Res Cardiol, 2011. **106**(5): p. 709-33.

67. Rojas, M., et al., *Bone marrow-derived mesenchymal stem cells in repair of the injured lung.* Am J Respir Cell Mol Biol, 2005. **33**(2): p. 145-52.

68. Lee, J.W., et al., *Therapeutic effects of human mesenchymal stem cells in ex vivo human lungs injured with live bacteria.* Am J Respir Crit Care Med, 2013. **187**(7): p. 751-60.

69. Busby, L.P., J.L. Courtier, and C.M. Glastonbury, *Bias in Radiology: The How and Why of Misses and Misinterpretations.* Radiographics, 2018. **38**(1): p. 236-247.

70. Cavanaugh, D., et al., *Quantification of bleomycin-induced murine lung damage in vivo with micro-computed tomography.* Acad Radiol, 2006. **13**(12): p. 1505-12.

71. *Common Terminology Criteria for Adverse Events (CTCAE) Version 5.0*, U.S.D.o.H.a.H. Services, Editor. 2017.

72. Pavy, J.J., et al., *EORTC Late Effects Working Group. Late Effects toxicity scoring: the SOMA scale.* Int J Radiat Oncol Biol Phys, 1995. **31**(5): p. 1043-7.

73. Veiga, C., et al., *Novel CT-Based Objective Imaging Biomarkers of Long-Term Radiation-Induced Lung Damage.* Int J Radiat Oncol Biol Phys, 2018. **102**(4): p. 1287-1298.

74. Coates, J., et al., *Contrasting analytical and data-driven frameworks for radiogenomic modeling of normal tissue toxicities in prostate cancer.* Radiother Oncol, 2015. **115**(1): p. 107-13.

75. Perez, J.R., et al., *A comparative analysis of longitudinal computed tomography and histopathology for evaluating the potential of mesenchymal stem cells in mitigating radiation-induced pulmonary fibrosis.* Sci Rep, 2017. **7**(1): p. 9056.

76. Krzywinski, M., *Image Color Summarizer 0.76*. 2006.

77. Buzug, T.M., *Computed Tomography, From Photon Statistics to Modern Cone-Beam CT*. 1 ed, ed. T.M. Buzug. 2008, Berlin: Springer-Verlag Berling Heidelberg. XIV, 522.

78. Schmitz, R.E. *Bioengineering 508: Phyiscal Aspects of Medical Imaging*. in *Bioengineering 508*. 2006. University of Washington: Imaging Research Laboratory.

79. Broder, J., *Imaging of Nontraumatic Abdominal Conditions*, in *Diagnostic Imaging for the Emergency Physician*. 2011. p. 445-577.

80. Oh, S. and S. Kim, *Deformable image registration in radiation therapy*. Radiat Oncol J, 2017. **35**(2): p. 101-111.